UNIVERSITY POLITEHNICA OF BUCHAREST

DOCTORAL SCHOOL OF ELECTRICAL ENGINEERING

PhD THESIS

SUMMARY

Metrics and tools to quantify the signals variability for power systems

Ing. Anca Petruța BRÎNCOVEANU

Scientific Coordinator: prof. dr. ing. Mihaela Marilena ALBU

Keywords: electrical measurements, statistical metrics, high reporting rates, voltage variability, frequency assessment

CONTENT

Introduction

The digitization and the trend towards energy efficiency of household and office appliances, along with the overall increase in the susceptibility of equipment, have led to a continuous interest from both the electricity provider and the consumer in the quality of electrical power. This interest has driven the search for efficient solutions to improve quality. An important step in this direction is the monitoring of quality indicators of the power supply. Thus, nowadays, power quality monitoring is an established field of research and application in the energy distribution sector. Moreover, power quality monitoring is highly standardized. However, due to the ongoing evolution of electrical distribution networks and the equipment provided, many aspects related to power quality remain debatable.

1 Variability of phenomena in power systems

1.1 Signals variability

The duration of signals associated with phenomena in energy systems divides these phenomena into: transient, stationary, and quasi-stationary.

Transient phenomena are characterized by rapid and temporary changes in the parameters of the energy system, such as voltage or electric current. They occur during events such as the sudden start-up or shutdown of electrical devices or during external disturbances, such as short circuits. Transient phenomena have a short duration and can have either temporary or permanent effects on the system, depending on their magnitude and duration. Transient phenomena in energy systems can pose risks to the equipment and infrastructure of these systems. Electrical protections are used to detect and respond to these phenomena promptly and effectively, in order to minimize the risk of damage or imbalances in the electrical networks [1].

Stationary phenomena in which the parameters of the electrical energy system remain relatively constant over time. For example, during the regular operation of an electrical system, when no major disturbances occur, parameters such as the effective value of voltage and the effective value of current can remain stationary for long periods of time. Stationary phenomena are fundamental for the evaluation and design of energy systems, as they represent the equilibrium or normal operating conditions of these systems. Stationary phenomena in energy systems represent conditions of equilibrium or stability in the operating quantities of the system, such as voltage, current, and power. Controlling these stationary phenomena is crucial for ensuring efficient and reliable operation of electrical networks.

1.2 Measurement and estimation of power quality parameters

The digitalization and energy efficiency of household and office appliances, along with the overall increase in equipment susceptibility, have led to a continuous interest from both the electricity provider and the consumer in the quality of electricity supply [2]. This interest drives the search for effective solutions to improve quality. An important step in this direction is the monitoring of quality indicators of the electricity supply [3]. Thus, nowadays, quality monitoring of energy is an established field of research and application in energy distribution. Additionally, energy quality monitoring is very well standardized.

1.2.1 Rapid Voltage Change - RVC

Rapid voltage changes are generally identified using data obtained from dedicated PQ meters [4]. The definition of RVC can be found in the IEC standard [5]: "An RVC event is defined in 3.26 and is generally a sudden transition between two steady-state voltages. The two steady-state voltages must be 'stationary,' a condition which is defined by the method below."

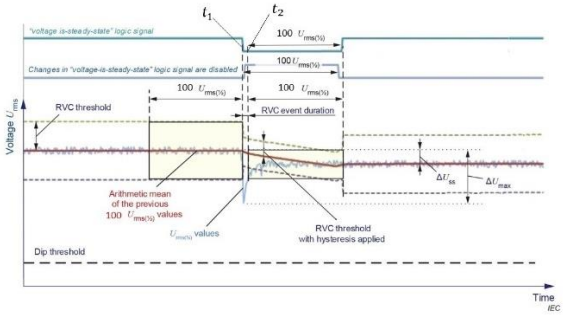

Figure 1.1 RVC event [5]

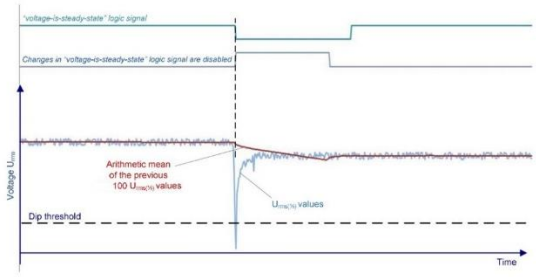

Figure 1.2 No RVC event [5]

In Figure 1.1, an RVC event is depicted, and several parameters are illustrated, such as: the duration of the event, which is the time between the moment the RVC event starts (t_1) and the moment the RVC event ends (t_2); the RVC threshold and the RVC threshold with hysteresis; ΔU_{SS} - the absolute value of the difference between subsequent steady-state RMS voltages; ΔU_{max} - the maximum absolute difference between any of the $U_{rms(1/2)}$ values during the RVC event and the arithmetic mean U_{mean} before the RVC event detected at moment t_1. The logical signal "voltage-is-stationary" is also represented in the figure in green. In Figure 1.2, an no RVC event is depicted.

1.2.2 IEC 61000-4-30 3rd edition vs IEC 61000-4-30 4th edition

To see and understand the differences between the algorithm from the 3rd edition and the algorithm from the 4th edition of the IEC 61000-4-30 standard, I have created two pseudocodes included in the thesis.

1.3 Measurement Systems

1.3.1 Power Quality Analyzers

Power quality analyzers are microprocessor-based measuring devices. They have the capability to measure voltage, current, frequency, phase shift, power factor, and power (active, reactive, and apparent) in electrical networks. These devices can monitor sags, interruptions, flicker, and rapid voltage changes [2].

1.3.2 Phasor Measurement Units -PMU

Phasor Measurement Units (PMUs) are specialized devices that perform measurements, monitor, and analyze the characteristics of voltage signals in an electrical network. They operate at a high reporting rate of up to 100 frames per second and use an external time source for high precision synchronization. In addition to measuring the effective values of voltage, PMUs are also capable of providing information about the phase of these quantities in real-time.

1.3.3 Micro-Phasor Measurement Units -µPMU

Micro-Phasor Measurement Units (µPMU) provides synchronized time measurements of dynamic energy flows in distribution networks and microgrids affected by Distributed Energy Resources (DERs). The microPMU is ideal for projects that require real-time network stability monitoring and provides a comprehensive view of the network at high resolution, with high accuracy of phase angle measured in milliradians.

1.3.4 Smart meters

The smart meter is typically viewed as an electrical energy measuring device that records information at preset time intervals. This data is sent to a data management center (usually a data concentrator) via bidirectional communication systems for monitoring and billing. The smart meter has

the advantage of being able to communicate directly with both the electricity provider and the consumer through a computer or mobile devices.

2 Relevant signals and systems in the measurement process

A signal is a phenomenon that represents information. Signals can be mathematically represented as elements of a set.

Deterministic signals are those that can be fully described by a (unique) explicit mathematical expression, a data table, or a well-defined rule. Deterministic signals include periodic signals - harmonic or non-harmonic and aperiodic signals: quasiperiodic and stationary signals.

Random signals are those that cannot be described by explicit mathematical formulas, or such a description would be too complex in practical terms. The analysis of random signals employs statistical techniques—probability theory and stochastic processes.

2.1 Metrics for variability assessment

Let there be an event for which the statistical variability is described by a continuous random variable X, for which the dataset $\{x_i\}$ with $i = \overline{1,n}$ is available. For this event, we consider the random variable Y represented by the dataset $\{y_i\}$ with $= \overline{1,n}$ as the estimator.

Coefficient of variation of RMSE

The coefficient of variation of RMSE is obtained by dividing the root mean square error (RMSE) by the mean value of the estimated value. This metric serves as an indicator for evaluating the accuracy of the signal model (y_i) relative to the collected samples (x_i).

$$CV(RMSE) = \frac{1}{\bar{y}}\sqrt{\frac{\sum_{i=1}^{n}(x_i - y_i)^2}{n}} \tag{2.1}$$

where $\bar{y}$ is the mean of the model values y_i.

Coefficient of variation RMSD

The coefficient of variation (CV) of the Root Mean Square Deviation (RMSD) is a statistical measure that provides a normalized measure of the variability of RMSD values. The RMSD is often used in the context of assessing the difference between predicted (y_i) and measured values (x_i) [6].

$$CV(RMSD) = \frac{1}{\overline{y_p}}\sqrt{\frac{\sum_{i=1}^{n}(x_i - y_i)^2}{n}} \tag{2.2}$$

where $\bar{y}_p$ refers to an assumed model value representative for the selected process time window. CV(RMSD) is a generalization of CV(RMSE) to express the relative variability of the root mean square error. It is important to note that, in our case, they are similar metrics because the assumed model value $\bar{y}_p$ is also the mean $\bar{y}$ of the model samples y_i calculated on T_r; the choice of representative model value $\bar{y}_p$ depends on the context of application, for example it can be chosen the rated power of the grid connection.

Coefficient of determination (R^2)

The coefficient of determination, denoted as R^2, serves as a metric for assessing the predictive or evaluative performance of a linear regression model. It provides a normalized measure of how well the model fits the data. By incorporating additional estimated variables, the R^2 value increases, leading to an adjusted model that provides a more precise estimation of the proportion of variation. The coefficient of determination can take values from negative infinity to 1, depending on the interplay between the ground truth and the prediction model [7].

$$R^2 = 1 - \frac{\sum_{i=1}^{n}(x_i - y_i)^2}{\sum_{i=1}^{n}(y_i - \tilde{y}_i)^2} \tag{2.3}$$

where $\tilde{y}_i$ is the adopted model of the estimated parameter over an analysis time window $T_a > T_r$. This metric cannot be applied to steady stated processes exhibiting no variability on T_a.

2.2 Correlations

Correlation is a statistical measure that expresses the degree of relationship between two variables. It indicates whether and to what extent the variation in one variable is associated with the variation in the other variable. Correlation can be positive (both variables increase together), negative (one variable increases while the other decreases), or close to zero (no obvious relationship). There are several types of correlation coefficients, with two of the most well-known being the Pearson correlation coefficient and the Spearman rank correlation coefficient.

Correlation analysis can provide insights into how changes in one time series are associated with subsequent or preceding changes in another time series.

The statistical concepts presented will be adapted and used to assess the variability of the power system by analyzing the main parameters of the system, namely voltage, frequency, and power.

3 Voltage variability

The process of measuring the variation of the parameters that characterize a signal is equivalent to a matching problem, where the mathematical equation is based on the agreed model of the physical phenomenon to which the signal is associated. Regardless of how an experimental determination is made, if we define a unit of measurement and a scale and then further consider estimating the Goodness of Fit [8] as a measure of model discrepancies from the reality (as described by the acquired samples), we will be able to notify the end user about potential deviation from the assumed model during the reporting time interval.

Steady-state voltage measurements in legacy LV power systems assume a periodical waveform of known frequency for which the root mean square (rms) value is selected as information carrier. Further, the signal model is assumed to be known and unique during the measurement time (T_w) and during the further aggregation time interval (T_a). According to the standard IEC 61000- 4-30 [5], most used value for T_w is 200 ms while windows of 3 seconds, 10 min and 2 hours respectively are considered for reporting an aggregated value (using a mean square formula).

Another option is to identify a signal matching metric to help quantifying the variability of the system in the current point of operation [9]. If such a metric is identified, the user will be able to estimate when the system is operating like the adopted model for the measurement.

In the following, we will consider standard signal models for LV distribution grids and define variability metrics based on T_w,T_a, and f_s, where f_s is the sampling frequency used by the respective digital measurement system. We make the hypothesis that, at least for the duration equal to T_a, all acquired samples are stored by the measurement system and can be used for both the signal model reconstruction and the computation of proposed indicators. Several aggregation windows have been considered and two sample rates for the acquired signals used to illustrate the method. The effect of pre-processing techniques (filtering) in the measurement chain have been neglected, and the acquired signal is supposed to reflect the energy transfer in the analyzed part of the grid.

3.1 Goodness of Fit

The measurement process is adequately performed when the information to be transferred from the analyzed phenomena is matching the quality of the measurement devices. Usually, classic measurements in for power systems this is equivalent to the premise of a steady state phenomenon during measurement time. This translates into a model with a few parameters that must be identified during measurement. Therefore, associating a metric to the assumed signal model will help acquiring more information on the phenomenon [10].

A method is proposed for assessing the variability of the electric power system using statistical metrics.

Let’s consider the model of alternate voltage described by the signal function y(t):

$$y(t) = U\sqrt{2}\,sin(2\pi ft + \varphi_0) \tag{3.1}$$

where the parameters able to fully describe the voltage:

$U \rightarrow$ rms value estimated on the measurement window T_w

$f \rightarrow$ system frequency (e.g., implicitly assumed to be 50 or 60 Hz)

$\varphi_0 \rightarrow$ initial phase estimated from a chosen time reference for a selected / commonly agreed reference framework.

In a digital voltmeter with sampling frequency $f_s \gg f$ the parameter (rms value over the measurement time T_w) is calculated from the samples of the acquired signal using the following sequence of formulas:

$$x_k = x(t_k)$$
$$y_k = U\sqrt{2}sin(2\pi f t_k + \varphi_0)\ ;\ \mathrm{k} = 1 \div \mathrm{N}_w$$
$$\mathrm{N}_w = [f_s/f]$$
$$U = U_{model}$$

where t_k is the sampling moment, N_w is the number of samples in T_w, y_k is the k–sample of the assumed implicit model for the measured signal and x_k is the k–sample of the acquired voltage signal.

In Figure 3.1 an example for T_w=2T_0 with T_0 the fundamental period of the voltage, in which both the implicit (sinusoidal) model and the (here, emulated) measurement signal are presented.

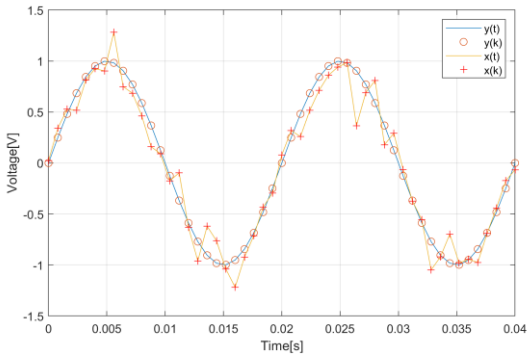

Figure 3.1 Example of the comparison between the implicit model $y(t)$ and the measured signal $x(t)$

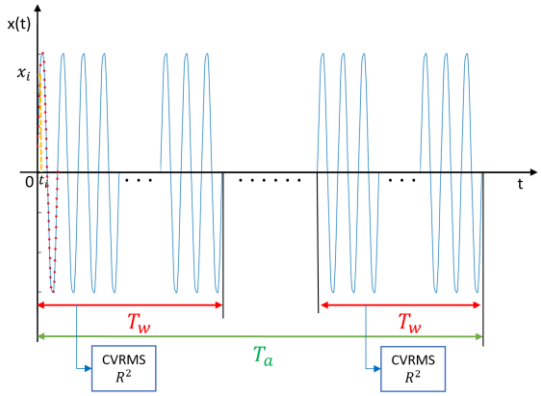

Figure 3.2 Example of time intervals succession

In Figure 3.2 an example for better understanding of T_w, T_a succession for the acquired signal x and the samples x_k used for computation of various metrics related to the deviation from the assumed model $y(t)$.

For voltage measurements, we apply CV(RMSE) to assess the adequacy of the signal model $y[i] = y_i$ with $y_i = y(\mathrm{i}/f_s)$, to the samples acquired during measurement: $x[i] = x_i; n = T_w/f_s$. For LV grids, the normalization can be done using either the rated value U_n, the actual rms value over the measurement time interval T_w or the actual rms value over the reporting time interval $T_a > T_w$. We selected $\bar{y} = \frac{\sum_{i=1}^{n} y_i}{T_w}$ where y_i are the samples in T_w.

$$CV(RMSE) = \frac{1}{\bar{y}}\sqrt{\frac{\sum_{i=1}^{n}(x_i - y_i)^2}{n}} \tag{3.2}$$

For voltage measurements, we apply R^2 to evaluate the adequacy of the signal model $y[i] = y_i$ to the samples $x[i] = x_i$ acquired during measurement window T_w.

$$R^2 = 1 - \frac{\sum_{i=1}^{n}(x_i - y_i)^2}{\sum_{i=1}^{n}(y_i - \tilde{y}_i)^2} \tag{3.3}$$

where $\tilde{y}_i$ is the mean value of y_i on T_{ss}.

For the mean value $\tilde{y}$ of the model, we consider the "best estimation" during a time interval T_{ss}, usually larger than the reporting time T_a, while T_{ss} is defined by the user as a time interval for which a steady state validity of the model is assumed. We have adopted $T_{ss} = T_a = 3\ s$ and therefore U_{Ta}, f, φ are the estimates for T_a:

$$\tilde{y}_i = U_{Ta}\sqrt{2}\ \sin(2\pi f t_i + \varphi) \tag{3.4}$$

In equation (3.3) to reduce the errors produced by zero division, we have rounded $|y_i - \tilde{y}_i|$ by the Δx_{max} corresponding to the declared quality for the measurement system:

$$|y_i - \tilde{y}_i| = \max(|y_i - \tilde{y}_i|, \Delta x_{max}) \tag{3.5}$$

Case study

To observe the characteristics of the energy transfer in a LV weak grid and see if we are in a steady state, we extract data sets with Elspec PQ analyzer, an equipment [11] enabling data acquisition on 16 bits, with high frequency sampling rate and making available the samples.

To acquire the experimental data, two different 10-minutes tests were carried out to observe voltage parameters variability during several durations of T_w and T_a. Data has been acquired for two different frequency sampling rates: $f_{s1} = 6400$ samples/s, $f_{s2} = 51200$ samples/s.

To test the metrics algorithms and their consistency, we use the signal x(t) acquired with the sampling frequency fs and compare its deviation from the implicitly assumed model y(t) for the voltage measurements corresponding to the energy transfer in a LV grid. For example, one signal model y[n] described by eq. (3.1) has the rms value of $x[n]$ computed over T_w=200 ms while frequency and phase depend on the level of detail with which we define the model.

In this case, for the acquired signal $x[n]$ the (synthesized) model $y[n]$ is described by (3.1). Here U is the rms value of x_i over T_w, f_{T_w} is the frequency estimated over T_w, U_{T_a} is the rms value of x_i over T_a, and f_{T_a}, is the frequency estimated over T_a, where the aggregation window is T_a=3 s.

$$\begin{aligned} U &= \sqrt{\frac{\sum_{i=1}^{n} x_i^2}{N_w}};\ N_w = f_s T_w; \\ f_{Tw} &= \begin{cases} \frac{10 \cdot f_s}{(c_{w+1} - c_1)} \\ \frac{10 \cdot f_s}{(c_w - c_1)} \end{cases}; \varphi_{Tw} = -\left(\frac{c_1}{f_s} - \frac{1}{4 \cdot f_{Tw}}\right) \\ \tilde{y}_i &= U_{Ta} sin\ (2\pi f_{Ta} t + \varphi_{Ta}) \end{aligned} \tag{3.6}$$

where c_k is the index of the i[th] maximum in the signal x_i in window T_w, $k = \overline{1, w}$, $w = length(T_w)$.

The initial phase has been estimated from the acquired samples, detecting the occurrence of the positive maxima, similarly to the PMU approach. [12].

Table 3.1 presents the results obtained after applying the previously presented metrics for $x[n]$, for two different sampling rates.

One can observe high values (compared to the reference ones) for MSE and MASE, despite the small deviation of the signal from the assumed model (see Figure 3.3), which makes the application difficult for real LV grids.

Moreover, the two indicators: CV(RMSE) and R^2 can discriminate between the assummed models (rated frequency versus estimated frequency), without introducing an extreme penalization for the model adequacy. Therefore, we choose to further apply only these two metrics CV (RMSE) and R^2.

To test the variability of the voltage signal (compared to the model adopted as a sinusoidal waveform with constant frequency and rms value), we applied the selected two metrics for each interval T_w =200 ms within T_a=3 s window. Table 3.2 presents R^2 for two different sampling rates applied to the voltage signal $x[n]$.

Table 3.1 Results obtained by applying metrics to a voltage signal x[n] acquired in a LV network for T_w=200 ms

Metrics	**Case 1 f=50 Hz** (f_{s1})	**Case 2 f=50 Hz** (f_{s2})	**Case 3** **f estimate from (12)** (f_{s1})	**Case 4** **f estimate from (12)** (f_{s2})
MAE	11.72	8.75	11.72	8.75
CV(RMSE)	0.06	0.04	0.05	0.04
…	….	…	…	…
MSPE [%]	2*10^6	1*10^7	2*10^6	1*10^7
$\boldsymbol{R^2}$	0.98	0.99	0.99	0.99
MASE	0.12	0.08	0.12	0.09

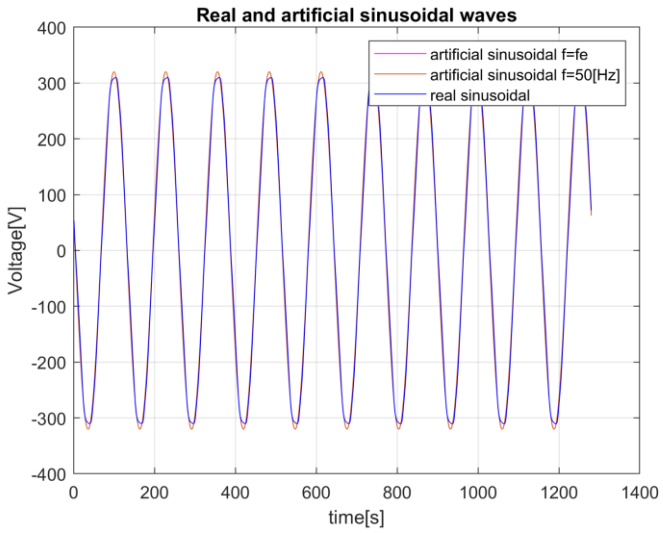

Figure 3.3 Voltage real signal $x_{11}[n]$ (red) and the model (blue)

Table 3.2 R^2 for voltage signal x[n] acquired with two sample rates on T_a = 3 s

Nr.	**Case 1** (f_{s1})	**Case 2** (f_{s2})
1	0.9981	0.9988
2	0.9980	0.9988
…		
15	0.9946	0.9947
max	0.9981	0.9988

As expected, higher sampling rates contribute to a higher degree of closeness to the adopted model (R^2closer to the reference/ideal value 1). Also, one can identify signal segments (of duration T_w) where the deviation from the model is larger than in other measurement windows. This suggests the use of R^2 as a flag to be added to the measurement result (reported rms value of the voltage) signalizing potential high variability during T_a. Evaluation of R^2 on each T_w during T_a allows not only the identification of larger deviations from the model, but also the localization of such events, where the acceptability for such variability within specified windows is user-selected by limits for R^2 or CV(RMSE). The former metric is more suitable to identifying large deviations from the model.

3.2 Synthetic signals – noise impact

As a further step in the study, to understand that R^2 can discriminate model inconsistency from measurement, we considered the same signal $x[n]$, corrupted by different levels of white noise (1 %, 0.5 %, 0.1 %) and then acquired using two sampling frequencies $f_{s1}$and f_{s2}.

In Figure 3.4, there are two signals: the ideal signal represented in red and the signal with 1% white noise represented in blue. In detail, we can see how the artificial signal is influenced by the noise.

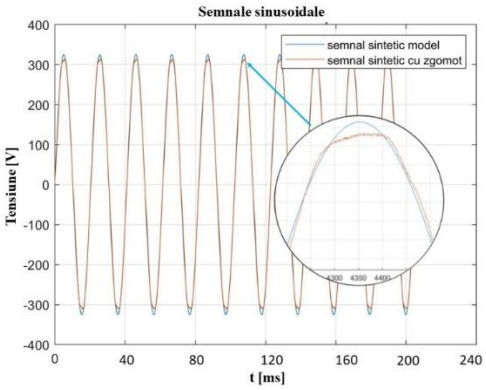

Figure 3.4 Signal $x[n]$ corrupted by white noise (1 %) and the corresponding model $y[n]$.

Table 3.3 presents the results for the two metrics obtained for $x[n]$ corrupted with three levels of white noise. The studied signal was acquired using two sampling rates, f_{s1} and f_{s2}. We observe that for the R^2 metric, the value is the same regardless of the level of white /noise applied to the signal, and the metric is not influenced by the sampling frequency. The CV(RMSE) values are influenced by the sampling frequency, and with a high sampling frequency, we can even identify the differences caused by a signal corrupted with 0.1% white noise.

Table 3.3 R^2 and CV(RMSE) for synthetic signal corrupted by noise

Metrics / noise level		**Obtain values**	
		f_{s1}	f_{s2}
CV(RMSE)	1 %	0.043	0.037
	0.5 %	0.043	0.035
	0.1 %	0.043	0.033
$\boldsymbol{R^2}$	1 %	0.998	0.998
	0.5 %	0.998	0.998
	0.1 %	0.998	0.998

3.3 RMS variability assessment

Deviations from the steady state model of the voltage signal in power system are currently quantified by the assessment of the RMS parameter and its profile during standardized time intervals. This assessment is done using Rapid Voltage Changes (RVC) which are fast variations in voltage levels in electrical distribution systems [13]. They are of common occurrence, especially at the distribution level, and are expected to become more frequent [14] with the increasing integration of dynamic loads and renewable-based generators into smart grids [15]. While RVCs are generally less critical compared to other power quality (PQ) events such as dips, sags, and swells, they can still pose challenges due to their potential to disrupt the operation of generators control systems and electronic equipment [16] [17].

We adapted the metrics (2.11) - (2.20) to the measurements performed on the signal $x(t)$, corelated with every T_r=1/RR reported measurement value x_m, where RR is the selected reporting rate of the measurement system. The assumed signal model $y(t)$ during T_r is described by the samples y_i, $i = 1 \dots n$, where n is the number of samples available during T_r but not reported. We denoted with $\tilde{y}$ the "best estimation" of the model during a time interval T_{ss}, usually larger than the reporting time T_a, while T_{ss} is defined by the user as a time interval for which a steady state validity of the model is assumed. For those cases where the best estimation is the average of a constant value model $(y_i - \tilde{y}_i)$ we have rounded $|y_i - \tilde{y}_i|$ by the Δx_{max} corresponding to the declared quality for the measurement system. We denoted with $\bar{y}_p$ a presumed model value that serves as a representation for the designated process time window. When that this selected model is corresponding to the mean computed over the T_r; $\bar{y}_p = \bar{y}$. In many real life scenarios, the assumed model value, represented as $\bar{y}_p$, corresponds to the mean of the model samples y_i computed over T_a; the selection of the representative model value $\bar{y}_p$ relies on the specific context of application.

Based on previous experiences and assessments with the metrics (2.11) to (2.20) across multiple measurands and processes [18], and based on this wealth of information, we found that the CV(RMSD) metric (2.16) is most suitable for characterizing the behavior of the power system based upon voltage assessment. We apply this metric to question the variability of the RMS reported values of voltage measurements in LV network using several time windows for analysis.

The measurements are made available with 1s time resolution by an Unbundled Smart Meter (USM), whereas the model is established based on the mean calculated over the reporting time of legacy smart meters [19].

The following parameters have been used for the voltage assessment:

$$x_i = U_i; y_i = \frac{\sum_{i=1}^{N_r} U_i}{N_r}; \bar{y}_p = \frac{\sum_{i=1}^{N_a} U_i}{N_a}; \tag{3.7}$$

where U– is the reported RMS value (estimated from the voltage signal on T_{sm}= 1 s measurement time), $N_r = T_r/T_{sm}$, $N_A = N_r \cdot M$ $M = T_a/T_r$, i=1…N_a.

For this investigation, we chose three legacy smart meters with reporting time intervals of T_r= 15 minutes, 30 minutes, and 1 hour, respectively. The analysis is conducted over a daily observation window designated as T_a=24 hours. To emphasize the continuous sequences of T_r and T_a in relation to the computation of various metrics assessing the deviation from the assumed model $y(t)$, an illustrative example is depicted in Figure 3.5.

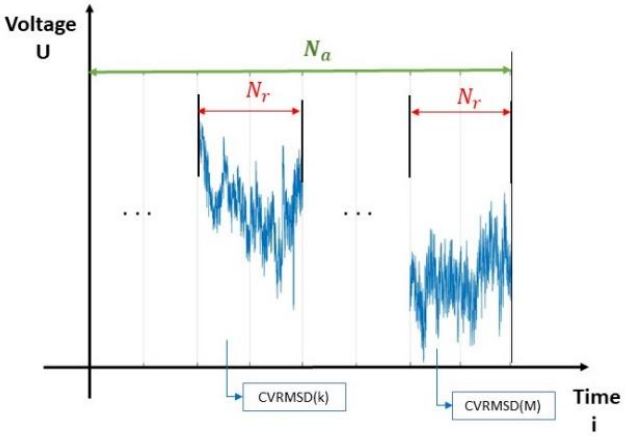

Figure 3.5 Time intervals for voltage (RMS values, computed on 1 s time window) variability assessment

We assess the voltage variability on a 3 phase LV network, where we note the RMS values on each phase as U_{k}, $k = \overline{1,3}$, during a summer day in 2023. The CV(RMSD) metric is computed for three different measurements windows: 15 minutes, 30 minutes and 1 hour respectively, while the aggregation is performed on a T_a= 2 h window.

Figure 3.6 presents daily voltage profile for the first phase (U_1) on 21 July 2023, while Figure 3.7 presents the CV(RMSD) values computed for the signal in Figure 3.6 using T_r=1 h, T_a=2 h. It can be observed that the maximum value is 0.78 %, reported at the end of the T_{r21} window at 21:00. We repeat the procedure for the other two phases U_2 and U_3 , on 21 July 2023, and the CV(RMSD) results are presented in Table 3.4. In the table we observe that the maxim CV(RMSD) value for U_2 is 1.68 % depicted at 1:00. For U_3 the maxim value is 2.32 % at the end of T_{r16}.

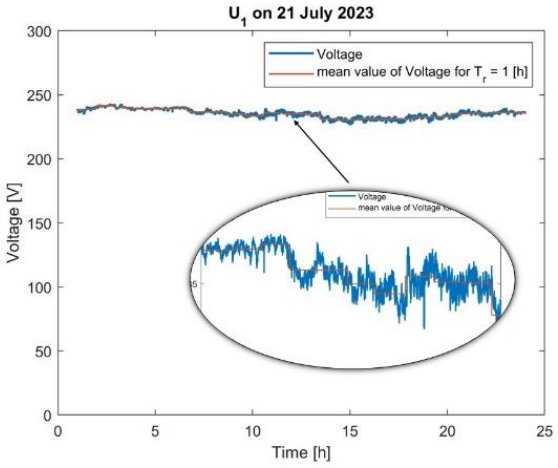

Figure 3.6 Voltage signal on phase 1 (U_1), on 21st July, measured value (blue), assumed constant model (red) on T_r=1 h

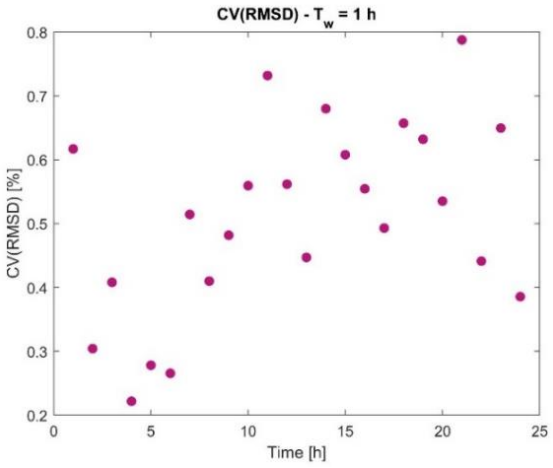

Figure 3.7 CV(RMSD) for the voltage U_1 in Figure 3.6

Table 3.4 CV(RMSD) for voltage (RMS values) on 21 st July 2023, T_r = 1 h

T_r	Reporting moment [hh:mm:ss]	CVRMSD for U_1 [%]	CVRMSD for U_2 [%]	CVRMSD for U_3 [%]
T_{r1}	[00:00:00-1:00:00)	6.17E-01	1.68E+00	1.70E+00
…	…	…	…	…
T_{r16}	[15:00:00-16:00:00)	5.54E-01	8.30E-01	2.32E+00
…	…	…	…	…
T_{r24}	[23:00:00-24:00:00)	3.86E-01	5.50E-01	3.95E-01

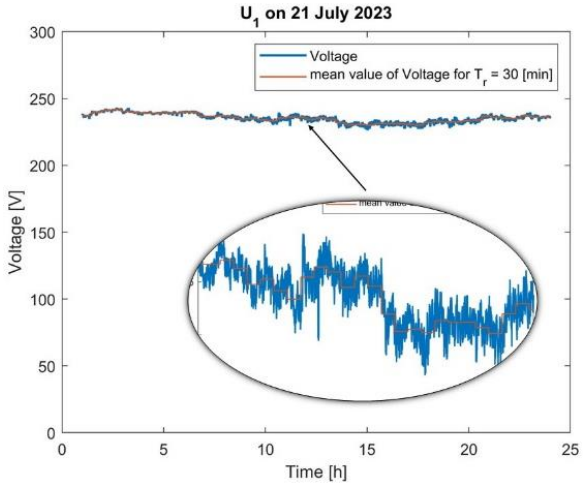

Figure 3.8 Voltage signal on phase 1 (U_1), on 21st July, measured value (blue), assumed constant model (red) on T_r= 30 minutes

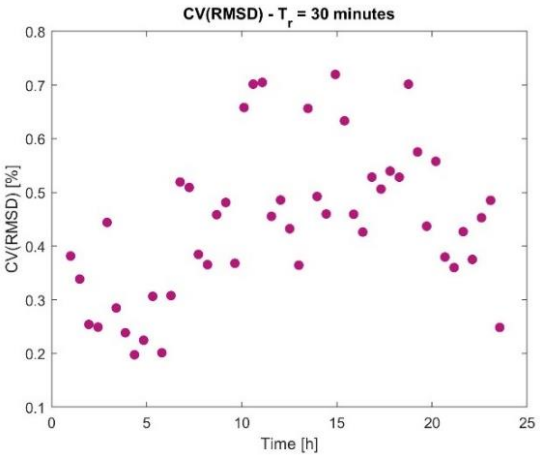

Figure 3.9 CV(RMSD) for the voltage U_1 in Figure 3.8

Figure 3.8 presents daily voltage profile for the first phase (U_1) on 21 July 2023, while Figure 3.9 presents the CV(RMSD) values computed for the same signal using T_r= 30 minutes, T_a=2 h. It can be observed that the maximum value is 0.72 % for reported window T_{r30}, at 15:00.

We repeat the procedure for the voltages on the other two phases (U_2, U_3), on 21 July 2023, with T_r = 30 minutes and the CV(RMSD) results are presented in Table 3.5, where we can observe that the maximum value is 2.34 % for U_2 and 2.57 % for U_3.

Table 3.5 CV(RMSD) for voltage (RMS values) on 21 st July 2023, T_r = 30 minutes

T_r	Reporting moment [hh:mm:ss]	CV(RMSD) for U_1 [%]	CV(RMSD) for U_2 [%]	CV(RMSD) for U_3 [%]
T_{r1}	[00:00:00-0:30:00)	3.82E-01	2.34E+00	2.37E+00
…	…	…	…	…
T_{r47}	[23:00:00-23:30:00)	4.85E-01	4.60E-01	2.37E-01
T_{r48}	[23:30:00-24:00:00)	2.48E-01	4.87E-01	3.35E-01

Figure 3.10 presents daily voltage profile for the first phase (U_1) on 21 July 2023, while Figure 3.11 presents the CV(RMSD) values computed for the signal in Figure 3.10 using T_r= 15 minutes, T_a=2 h. It can be observed that the maximum value is find in window T_{r21} at 10:15 and is 0.91 %.

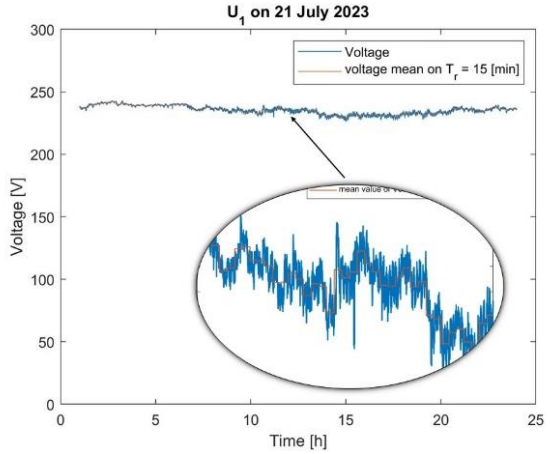

Figure 3.10 Voltage signal on phase 1 (U_1), on 21st July, measured value (blue), assumed constant model (in red) on T_r= 15 minute

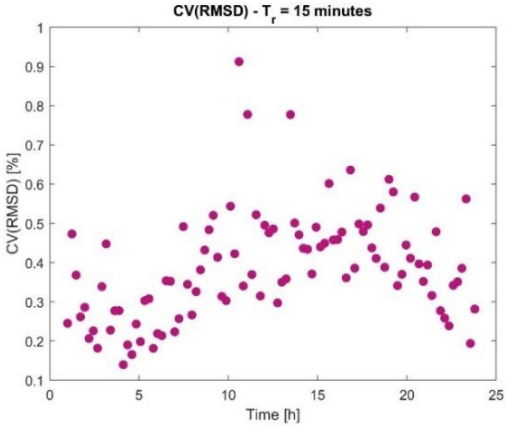

Figure 3.11 CV(RMSD) for the voltage U_1 in Figure 3.10

We repeat the procedure for the voltages on the other two phases (U_2, U_3), on 21 July 2023, with T_r = 15 minutes. a Results are presented in Table 3.6, where we can observe that the maximum value is 3.3% for U_2 and is 2.32 % and 3.28 % for U_3.

Table 3.6 CV(RMSD) for voltage (RMS values) during 21 July 2023, T_r = 15 minutes

T_r	Reporting moment [hh:mm:ss]	CV(RMSD) for U_1 [%]	CV(RMSD) for U_2 [%]	CV(RMSD) for U_3 [%]
T_{r1}	[00:00:00-00:15:00)	2.45E-01	3.30E+00	3.28E+00
…	…	…	…	…
T_{r41}	[10:00:00-10:15:00)	9.12E-01	7.86E-01	9.09E-01
T_{r42}	[10:15:00-10:30:00)	3.40E-01	4.73E-01	2.27E-01
…	…	…	…	…
T_{r96}	[23:45:00-24:00:00)	2.82E-01	2.85E-01	2.20E-01

To have a better overview on the voltage variability, we analyzed the voltage profile during one week in April 2023. For this assessment we perform the CV(RMSD) calculations with two reporting rates (1 frame per hour and 4 frames per hour) and T_a=2 h. We applied equation (2.16) considering that the presumed model value $\bar{y}_p$ is the nominal voltage ($\bar{y}_p = U_n$).

Table 3.7 presents the maximum and minimum CV(RMSD) values for one week, for the three-phase voltage signals (U_1, U_2, U_3), T_r= 1 h T_a=2 h. It can be observed that the maximum variability is on U_3 where CV(RMSD) equal with 3.38 % (Thursday, 08.04.2023). The minimum CV(RMSD) is 0.24 %, also on U_3 (Wednesday 07.04.2023).

Table 3.7 CV(RMSD) during one week in April, T_r = 1 h

Day	U_1		U_2		U_3	
	CV(RMSD), T_r=1 h					
	max [%]	min [%]	max [%]	min [%]	max [%]	min [%]
05.04.2023	1.86	0.41	1.88	0.34	3.09	0.4
06.04.2023	1.38	0.37	1.59	0.38	3.1	0.25
...	...	...	...	...	...	...
11.04.2023	1.19	0.35	1.88	0.4	2.04	0.25

Table 3.8 presents the maximum and minimum CVRMSD values for one week, for the three-phase voltage signals (U_1, U_2, U_3), T_r= 15 minute, T_a=2 h. It can be observed that the maximum variability is on U_3 where CV(RMSD) equal with 3.48 % (Monday, 05.04.2023). The minimum CV(RMSD) is 0.16 %, also on U_3 (Saturday 10.04.2023).

Table 3.8 CV(RMSD) during one week in April, T_r = 15 minutes

Day	U_1		U_2		U_3	
	CV(RMSD), T_r=15 min					
	max [%]	min [%]	max [%]	min [%]	max [%]	min [%]
05.04.2023	1.48	0.22	1.85	0.21	3.48	0.2
06.04.2023	1.55	0.26	2.16	0.18	2.61	0.17
...	...	...	...	...	...	...
11.04.2023	1.13	0.25	1.9	0.2	2.02	0.18

Further, to estimate the daily voltage variability with only one CV(RMSD) indicator we apply the equation (2.16) with nominal voltage as the presumed model value $\bar{y}_p$ and T_a=2 h:

$$y_i^* = \frac{\sum_{i=1}^{N_r} U_i}{N_r}; \bar{y}_p = U_n; \tag{3.8}$$

Results for the considered week in April, using the proposed model y_i^* (see Figure 3.12) are presented in Table 3.9. It can be observed that the highest CV(RMSD) value is on Thursday (08.04.2023) for U_3. Almost all week the CV(RMSD) value for this phase was bigger than 1.3 %, while for U_1 and U_2 the CV(RMSD) values were around 1 %, fact that highlights that on phase U_3 we have the greatest voltage variability.

Table 3.9 CV(RMSD) values for the assumed model y_i^* with T_r = 2 h, one week in April

Zi	CV(RMSD) for U_1 [%]	CV(RMSD) for U_2 [%]	CV(RMSD) for U_3 [%]
05.04.2023	0.96	1.15	1.38
06.04.2023	0.80	1.05	1.44
...	...	...	...
11.04.2023	0.79	1.05	1.39

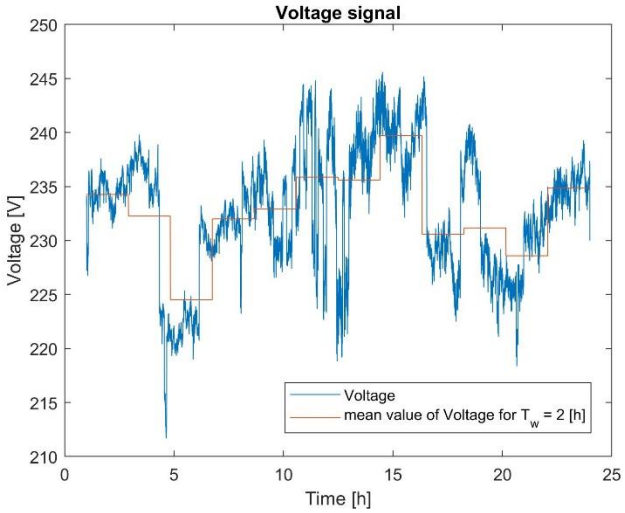

Figure 3.12 Voltage signal x_i (blue) and assumed model y_i^* (red)

The study carried out for the considered week in April provides important information about the assessment of system variability in the three-phase network based on information measurements.

Our interest is not the global variability of the RMS voltage parameter, but rather in its variability within the legacy reporting interval adopted by the power quality community. Our aim is to highlight that this reporting interval is no longer adequate.

Therefore, we seek to demonstrate the need for a revised reporting method to better capture the dynamics of modern electrical networks. The study was conducted on a network with specific characteristics, this affects the generalizability of the results, but our idea is to propose a method to quantify the system variability. We plan to extend our research to include a variety of network environments in future studies to validate the generality of the proposed metric CV(RMSD) applied on the RMS voltage values.

4 Frequency variability

The increasing number of users sensitive to disturbances requires more attention to be paid to the potential power quality (PQ) issues. However, in the power quality framework only signals characteristics to steady state operation of energy systems are considered. The higher share of RES-based electricity generation changes the boundary conditions discriminating between steady state and dynamic operational of emerging energy systems. Moreover, regulatory constraints and standardized requirements add difficulties to the appropriate selection of measurement devices to exactly identifying potential PQ issues. For example, the standard that defines not only the PQ parameters but also the context for their measurement is IEC 61000-4-30. According to it, the power quality analysis should be performed on the frequency signal done on aggregated measurement windows of 1 second, 10 seconds and 10 minutes [5], while the measurement information is obtained with the basic measurement time T_{PQ}=200 ms. The measurement basic time intervals must not overlap with each other and any individual cycles that extend beyond the 10-second time interval are discarded. Each 10-second interval will start precisely at a fixed 10-second time mark.

Recorded frequency measurements from the power system show an increase variability even in steady state conditions of operation. Therefore, it became needed to establish a framework to assess the frequency variation in a specified wide area network and estimate the information suitability to various steady state applications. Presently, the most accurate frequency measurements are provided by phasor measurements units (PMUs). A PMU provides a complex measurement data frame for voltages and currents in a power system node with high reporting rate (up to 100 frames/s), using a common time source for synchronization [20][21]. In this paper using PMU data we intend to develop guidelines for statistical analysis of frequency variation, based on two metrics: coefficient of variation of root mean squared error CV(RMSE) and coefficient of determination R^2. The signal model is assumed to be known and unique during the measurement time (T_w) and during the further aggregation time interval (T_a).

Let's consider a power system operating in steady-state conditions, for which the frequency information is provided with high reporting rates by PMUs. The steady state model for inertial power system is described by sinusoidal voltage signals:

$$u_m(t) = \hat{U}sin(2\pi ft + \varphi) \tag{4.1}$$

where: $f = constant = f_n$, on the observation interval T_{ss}; f_n – nominal frequency [Hz]; $\hat{U}$ – voltage amplitude [V]; $\varphi -$ initial phase angle and t – time.

Considering the large number of sources of variation for the parameters that characterize the energy transfer in large power systems, we base our analysis on metrics to be applied to the time series of measured frequency values: the coefficient of variation of root mean squared error and the coefficient of determination R^2. Basically, those metrics assess the distance between the frequency profile and the assumed model (constant frequency) over specified time windows.

$$CV(RMSE) = \frac{1}{\bar{y}}\sqrt{\frac{\sum_{i=1}^{n}(x_i - y_i)^2}{n}} \tag{4.2}$$

$$R^2 = 1 - \frac{\sum_{i=1}^{n}(x_i - y_i)^2}{\sum_{i=1}^{n}(y_i - \tilde{y}_i)^2} \tag{4.3}$$

$$x_i = f_i; y_i = \bar{y} = \frac{\sum_{i=1}^{N_w} f_i}{N_w}; \tilde{y}_i = \frac{\sum_{i=1}^{N_{ss}} f_i}{N_{ss}} = \tilde{y} \tag{4.4}$$

where: y_i – estimate value; x_i – measured value

The model is depicted by the variable y_i which has a constant value on T_{PQ}=200 ms window (following the PQ framework assumptions) while the frequency discrete signal depicting "the reality" is x_i , $i = \overline{1, N_w}$. For example, when x_i is provided by PMUs with a 50 frames/s reporting rate, which is equivalent to a reporting time T_r= 20ms, the number of samples is N_w=T_{PQ}/T_r=10 (see Figure 4.1).

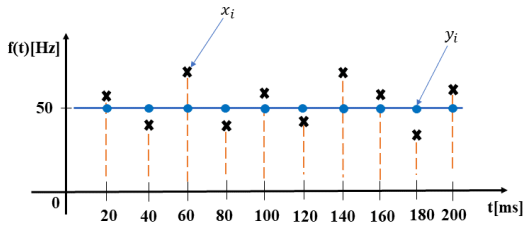

Figure 4.1 Model example for T_{PQ} =200 ms, T_r =20 ms, N_w=10 , y_i=f_n=50 Hz

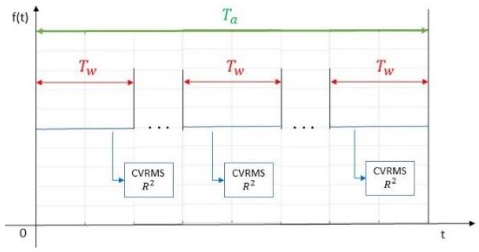

Figure 4.2 Example of time intervals for frequency analysis

To better understand the succession of T_w and further aggregation T_a for the acquired signal x_i to compute various metrics related to the deviation from the assumed model y_i, let's consider the example for Figure 4.2.

To test the usefulness of the proposed metrics we firstly generate a synthetic frequency signal x_i^*, uniformly distributed with mean = 50 Hz and standard deviation 5,77 mHz. The signal is represented in Figure 4.3 and the goal is to compare it with the model y_i. In this case the steady state model is:

$$y_i = \bar{y} = \frac{\sum_{i=1}^{N_r} x_i^*}{N_r}; \tilde{y}_i = \frac{\sum_{i=1}^{N_{ss}} x_i^*}{N_{ss}};$$

The metrics are computed for two cases corresponding to $T_w = 1\ s$ and $T_w = 200$ ms respectively considering T_{PMU}= 20 ms, T_a=10 s, N_a=500; T_{ss}=10 min, N_{ss}=30000. Table 4.1 gives the values of R^2 and CV(RMSE), computed for x_i^* on $T_w = 1\ s$ corresponding to 600 values of $T_{w,i}$ in the observation interval $T_{ss} = 10$ minutes.

Table 4.2 gives the values of R^2 and CV(RMSE), computed for x_i^* on $T_w = 200$ ms corresponding to 3000 values of $T_{w,i}$ in the observation interval $T_{ss} = 10$ minutes. One can observe that both metrics shown no significant deviation from the steady-state corresponding values; the maximum value of CV(RMSE) is 8.76E-04 while the minimum value of R^2 is 0.9923 both extremes being calculated for the window 1593, i.e., 318.4 s ≤ t <318.6 s.

Table 4.1 Metrics of synthetic frequency x_i^* for T_w= 1 s

i	Metrics on $T_{w,i}$	
	CV(RMSE)	R^2
1	1.08E-04	1.0000
2	1.08E-04	1.0000
…	…	…
319	5.01E-04	0.9974
…	…	…
600	1.21E-04	1.0000

Table 4.2 Metrics of synthetic frequency x_i^* for T_w=200 ms

i	Metrics on $T_{w,i}$	
	CV(RMSE)	R^2
1	1.07E-04	1.0000
2	1.16E-04	1.0000
…	…	…
1593	8.76E-04	0.9923
…	…	…
3000	1.39E-04	1.0000

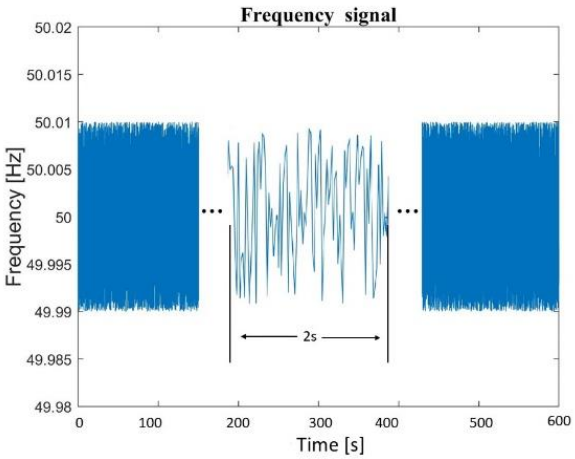

Figure 4.3 Emulated frequency variation for $T_{ss} = 10$ minutes signal x_i^*

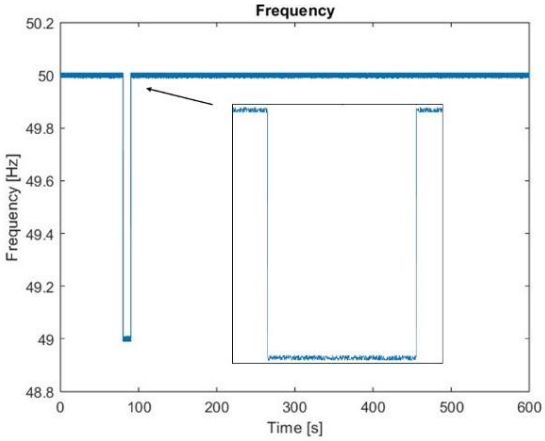

Figure 4.4 Emulated frequency variation for $T_{ss} =$ 10 minutes signal x_i^{**}

We repeat the procedure for the same synthetic signal x_i^* to which a perturbation of 200 ms is imposed, resulting x_i^{**} (see Figure 4.4).

Table 4.3 gives the values of R^2 and CV(RMSE), computed for x_i^{**} on $T_w = 1\ s$, corresponding to 600 values of $T_{w,i}$ in the observation interval $T_{ss} = 10$ minutes. One can see that the event has been identified by the 80th analysis window $T_{w,80}$ (79 s ≤ t< 80 s), where CV(RMSE) maximum value is 0.0028 and R^2 minimum value is 0.922.

Table 4.3 Metrics of synthetic frequency x_i^{**} for T_w= 1 s

i	Metrics on $T_{w,i}$	
	CV(RMSE)	R^2
1	1.079E-04	0.9999
…	…	…
80	28E-04	0.9222
…	…	…
600	1.207E-04	0.9999

Table 4.4 Metrics of synthetic frequency x_i^{**} for T_w=200 ms

i	Metrics on $T_{w,i}$	
	CV(RMSE)	R^2
1	1.07E-04	0.9999
…	…	…
400	60E-04	0.6433
…	…	…
3000	1.38E-04	0.9998

Table 4.4 gives the values of R^2 and CV(RMSE), computed for x_i^{**} on $T_w = 200$ ms corresponding to 3000 values of $T_{w,i}$ in the observation interval $T_{ss} = 10$ minutes. One can see that the event has been better localized by the 400th analysis window $T_{w,400}$ (79.8 s ≤ t<80 s), where CV(RMSE) maximum value is 0.006 and R^2 minimum value is 0.6433.

4.1 Frequency signal available with 50 frames/s reporting rate

We analyze the frequency variation using data acquired with a high reporting rate (50 frames/s) using a PMU, equipment, placed in the university laboratory MicroDERLab [22] which measures the frequency with a precision of 10^{-6}. In this evaluation, the two metrics CV(RMSE) and R^2 [7] are applied for the frequency signal (f_i).

To obtain the desired results, we will use formulas (2.7) - (2.16) in which we will substitute the parameters used for a 1 s window:

T_w= 200 ms, T_a=1 s, T_{ss}=10 min, N_w=10; N_a=50; N_{ss}=30000.

T_w – measurement window, T_a – aggregation window, T_{ss}- steady-state window, defined by user

By applying the metrics to large datasets, we can identify cases with small frequency variations (within the T_w window and using the averaged frequency model over the T_a window) or we can identify events where the signal may deviate more than 10% from the frequency model, considered constant and ideal. Figure 4.5 and Table 4.4 present a case with small frequency variations. In this graph, it can be observed that the lowest value is 49.7 Hz, reaching the lower limit imposed by 6 % of the nominal frequency (50 Hz). In Table 4.4, we can see that the largest deviation from the ideal model occurs in the window [$2T_w \ldots 3T_w$].

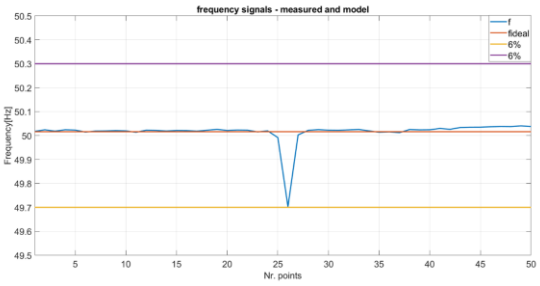

Figure 4.5 Small frequency variation (x[n] – blue) and the model with constant frequency (y[n] – red)

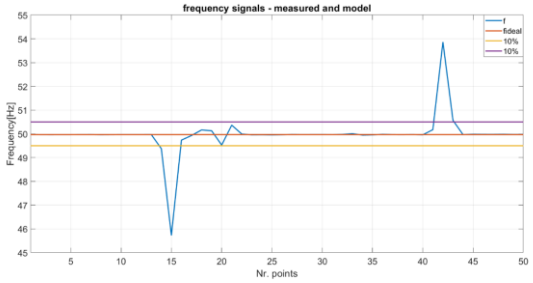

Figure 4.6 Large frequency variation (x[n] – blue) and the model with constant frequency (y[n] – red)

Table 4.3 R^2 and CV(RMSE) for a frequency signal with small variability for T_a =1 s, T_w =200 ms

Nr.	**Metrics**		
	CV(RMSE)	R^2	
		$\varepsilon_{max} = 2E-03$	$\varepsilon_{max} = 2E-06$
[0…T_w]	6.86E-05	9.99E-01	7.35E-01
…	…	…	…
[4T_w …T_a=5T_w]	1.42E-04	9.95E-01	-1.50E+00

Figure 4.6 and Table 4.5 present an example where there are large frequency variations. In this graph, we observe that there are large frequency variations exceeding the 10 % limit, concluding that this variation represents an event. In Table 4.6, we can see that there are two windows with large frequency variations [$T_w \ldots 2T_w$] and [$4T_w \ldots T_a$=$5T_w$].

Table 4.4 R^2 and CV(RMSE) for a frequency signal with large variability for T_a =1 s, T_w =200 ms

Nr.	**Metrics**		
	CV(RMSE)	R^2	
		$\varepsilon_{max} = 2E-03$	$\varepsilon_{max} = 2E-06$
[0…T_w]	4.09E-05	1.00E+00	1.00E+00
…	…	…	…
[4T_w …T_a=5T_w]	3.54E-03	-2.14E+00	-3.14E+06

4.2 Frequency signal available with 25 frames/s reporting rate

The frequency variation analysis is performed on datasets acquired with a high reporting rate (25 frames/s), using PMUs, equipment that measures frequency with a precision of 10^{-6} Hz. These data are obtained from a network of phasor measurement units (PMUs) located in 13 different substations in Romania, connected to the 400 kV network, a network implemented by Transelectrica in 2009.

We aim to observe the capability of the metrics to identify events by applying them to data acquired during power system faults that occurred in 2018 and 2017. To obtain the desired results, we will use formulas (4.1), (4.2), and (4.3) in which we will substitute the used parameters. For a 1 s window: T_w= 1s, T_a=10 s, T_{ss}=10 min, N_w=25; N_a=250; N_{ss}=15000. For a 200 ms window: T_w= 200 ms, T_a= 10 s, T_{ss}=10 min, N_w= 5; N_a= 50; N_{ss} = 15000.

In 2018, both units of the nuclear power plant (NPP) were operational, but unexpectedly, one of the units experienced a sudden disconnection. As a result of this action, 700 MW of generation capacity was lost, leading to a reduction of mechanical inertia to half of its total value [23].

Figure 4.7 shows the frequency variation recorded over a 10 minutes acquisition period. The legend displays each station in different colors.

Table 4.6 presents the minimum R^2 values and the maximum values for the remaining metrics for each city over a 10 minutes period with a 1-second measurement window. It is observed that the largest frequency deviation occurs at the Cernavodă station with an R^2 value of 0.98 and a CV(RMSE) of 0.000979.

Table 4.7 presents the minimum values for R^2 and the maximum values for the remaining metrics for frequency variation over a 10 minutes period, with a 200 ms measurement window. The Cernavodă station is the most affected by frequency variation with R^2 =0.98 and a CV(RMSE) of 0.000499.

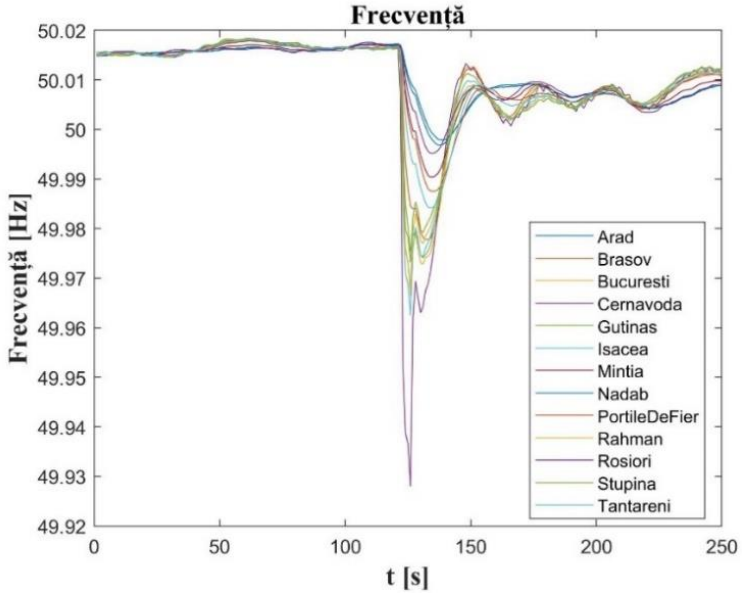

Figure 4.7 Frequency variation in different nodes in 2018

Table 4.5 Metrics for acquired data in 2018 on T_w= 1s

Node	Metrics: maxim from 600 de values on 10 minutes							
	MAE (max)	**MSE (max)**	**RMSE (max)**	**CV(RMSE) (max)**	**MAPE (max)**	**MSPE (max)**	**R^2 (min)**	**MASE (max)**
Bucuresti	1.27E-02	2.04E-04	1.43E-02	2.85E-04	4.34E-04	2.65E-11	9.99E-01	2.54E-02
Cernavoda	2.05E-02	5.87E-04	2.42E-02	4.84E-04	9.79E-04	7.65E-11	9.98E-01	4.10E-02
...	...	...	...	...	...	...	...	...
Tantareni	5.77E-03	4.52E-05	6.73E-03	1.34E-04	2.20E-04	5.89E-12	1.00E+00	1.15E-02

Table 4.6 Metrics for acquired data in 2018 on T_w= 200 ms

Node	Metrics: maxim from 3000 de values on 10 minutes							
	MAE (max)	**MSE (max)**	**RMSE (max)**	**CV(RMSE) (max)**	**MAPE (max)**	**MSPE (max)**	**R^2 (min)**	**MASE (max)**
Bucuresti	8.88E-03	1.25E-04	1.12E-02	2.23E-04	1.96E-03	1.95E-11	1.00E+00	1.78E-02
Cernavoda	1.98E-02	6.24E-04	2.50E-02	4.99E-04	8.98E-03	1.98E-10	9.98E-01	3.95E-02
...	...	...	...	...	...	...	...	...
Tantareni	3.13E-03	1.29E-05	3.59E-03	7.18E-05	1.30E-03	1.01E-11	1.00E+00	6.26E-03

In 2017, a significant energy loss led to a decrease in frequency, with the potential to affect system stability. The frequency variation was primarily caused by the previous disconnection of a high-power generator, which significantly reduced the mechanical inertia available in the power system of Romania.

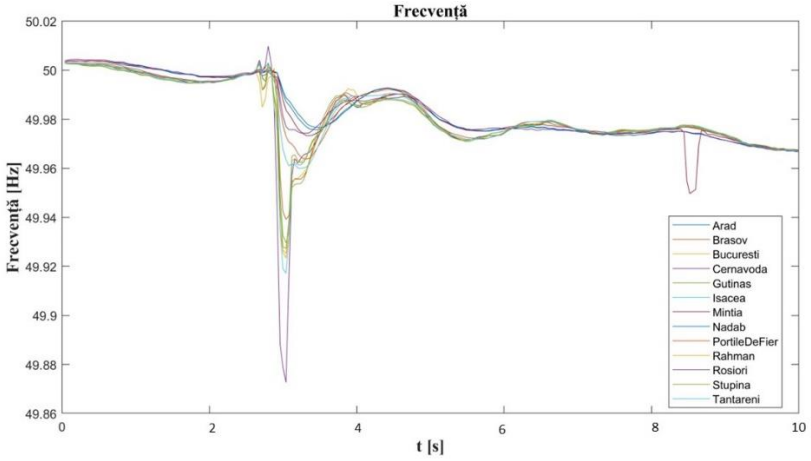

Figure 4.8 Frequency variation in different nodes in 2017

Figure 4.8 shows the frequency variation during this event at 13 different nodes of the transmission network in Romania, for an identical analysis window with a duration of T_{ss} =10 minute.

Table 4.7 Metrics for acquired data in 2017, T_w= 1 s

Node	Metrics: maxim from 600 de values on 10 minutes							
	MAE (max)	**MSE (max)**	**RMSE (max)**	**CV(RMSE) (max)**	**MAPE (max)**	**MSPE (max)**	**R2 (min)**	**MASE (max)**
Bucuresti	2.21E-02	6.26E-04	2.50E-02	5.01E-04	7.52E-05	1.54E-12	9.97E-01	4.43E-02
Cernavoda	2.90E-02	1.54E-03	3.92E-02	7.84E-04	8.64E-05	3.77E-12	9.94E-01	5.79E-02
...	...	...	...	...	...	...	...	...
Tantareni	1.75E-02	3.22E-04	1.79E-02	3.59E-04	5.63E-05	7.89E-13	9.99E-01	3.51E-02

Table 4.8 presents the minimum R^2 values and the maximum values for the remaining metrics for each station over a 10 minutes period with a 1 s measurement window, corresponding to 600 values. The table shows that the station most affected by the frequency variation is the Cernavodă node.

Table 4.8 Metrics for acquired data in 2017, T_w= 200 ms

Node	Metrics: maxim from 600 de values on 10 minutes							
	MAE (max)	**MSE (max)**	**RMSE (max)**	**CV(RMSE) (max)**	**MAPE (max)**	**MSPE (max)**	**R2 (min)**	**MASE (max)**
Bucuresti	2.98E-02	9.85E-04	3.14E-02	6.28E-04	1.04E-04	4.83E-13	9.96E-01	5.96E-02
Cernavoda	4.09E-02	1.92E-03	4.38E-02	8.76E-04	9.60E-05	9.43E-13	9.92E-01	8.17E-02
...	...	...	...	...	...	...	...	...
Tantareni	1.17E-02	1.61E-04	1.27E-02	2.54E-04	3.73E-05	7.91E-14	9.99E-01	2.34E-02

Table 4.9 presents the minimum R^2 values and the maximum values for the remaining metrics for frequency variation over a 10 minutes period, with a 200 ms measurement window, corresponding to 3000 values. We observe that the largest frequency deviation occurs at the Cernavodă station.

For a more detailed analysis of this case, we consider 4 nodes of the transmission network in Romania where the phasor measurement units (PMUs) are located, as shown in Figure 4.9.

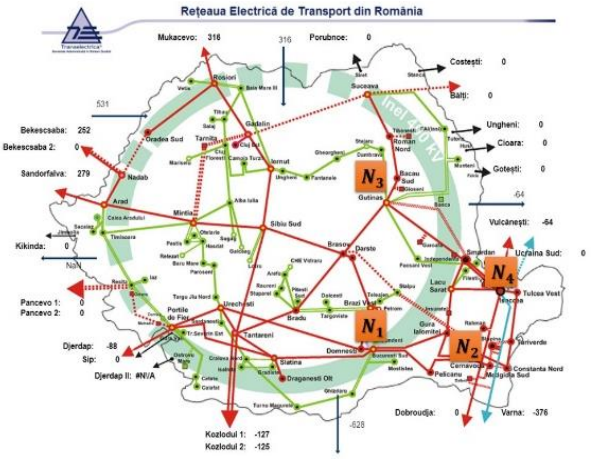

Figure 4.9 Romanian transmission network (400kV) modified after [24]

Figure 4.10 presents the frequency variation during this event, in four different nodes of the Romanian transmission system, for an identical analysis window of duration T_{ss} =10 minutes. Further we analysed the signal with the highest variability (node N_2). To study the impact of the event on the frequency signal we will apply the statistics metrics CV(RMSE) and R^2.

Table 4.10 gives the values of R^2 and CV(RMSE) on $T_w = 1\ s$ corresponding to 600 values of $T_{w,i}$ in the observation interval $T_{ss} = 10$ minutes. We observed that the variability is weakly identified in window $T_{w,319}$ (318 s ≤ t < 319 s).

In Table 4.11 gives the values of R^2 and CV(RMSE), computed on $T_w = 200$ ms corresponding to 3000 values of $T_{w,i}$ in the observation interval $T_{ss} = 10$ minutes. We observed that the frequency variation is identified in the window $T_{w,1594}$ (318.6 s ≤ t< 318.8 s).

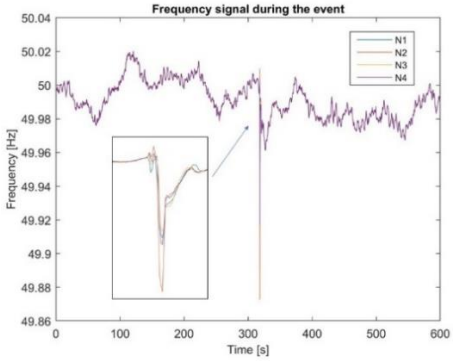

Figure 4.10 Frequency variation for the analyzed event, time counted from t=0

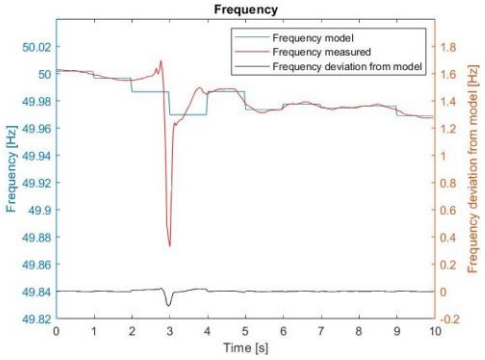

Figure 4.11 Frequency in N_2 during the event on T_{PMU}= 40ms, T_w= 1s, T_a=10s analysis window, time counted from t_1=313.64 s

Table 4.9 Metrics for frequency during event T_w= 1 s

i	Metrici pe $T_{w,i}$	
	CV(RMSE)	**R^2**
1	7.92E-06	0.9999
2	6.21E-06	1.0000
…	…	…
600	17.6E-06	0.9999

Table 4.11 Metrics for frequency during event T_w= 200 ms

i	Metrics pe $T_{w,i}$	
	CV(RMSE)	**R^2**
1	3.71E-06	1.0000
2	1.96E-06	1.0000
…	…	…
3000	1.60E-06	1.0000

To better highlight the frequency variability as detected by the proposed metrics we further analysed the difference between the signal f_i and a selected signal (model) for the case of pattern timeline of the T_a =1s. The selected pattern f_{model} is described by:

$$f_{model,i} = f_k^*, for\ N_w(k-1)+1 < i < kN_w$$
$$N_w = \frac{T_w}{T_{PMU}} = 25; \quad (4.5)$$
$$f_k^* = \frac{\sum_{N_w(k-1)+1}^{kN_w} f_i}{N_w}, k = \overline{1,10}$$

We denote the difference between the two signals as Δf_{model}:

$$\Delta f_{model} = f_i - f_{model} \quad (4.6)$$

In Figure 4.11 the acquired frequency in the substation N_2 during the event is compared with the imposed model. The difference Δf_{model} (where f_{model} is obtain by averaging the frequency in one second window) is also depicted in Figure 4.11.

The values of R^2, obtained for T_w= 1s, during the selected T_a =10 seconds are depicted in Figure 4.12. The values of CV(RMSE), obtained for T_w= 1s, during the selected T_a =10s are depicted in Figure 4.13. We repeat the analysis for the same signal in substation N_2 for a smaller analysis window T_w= 200ms (see Figure 4.14) and the frequency model f_k^* defined in (4.5) for $N_w = \frac{T_w}{T_{PMU}} = 5$.

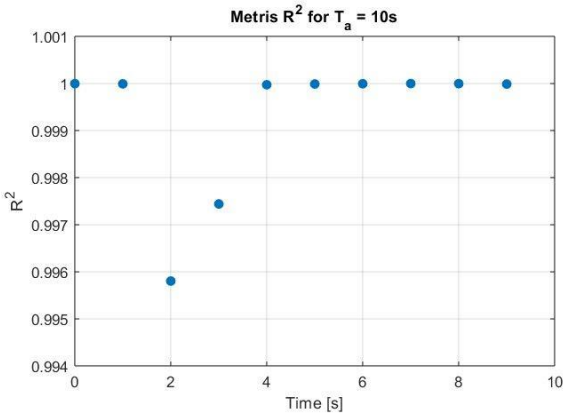

Figure 4.12 R^2 values calculated for the frequency signal during the event T_{PMU}= 40 ms, T_w= 1 s, T_a= 10 s, time counted from t_1=313.64 s

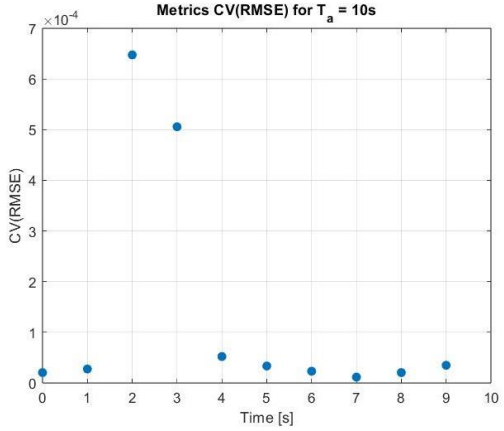

Figure 4.13 CV(RMSE) values calculated for the frequency signal during the event T_{PMU}= 40 ms, T_w= 1 s, T_a= 10 s, time counted from t_1=313.64 s

In Figure 4.14 the acquired frequency in the substation N_2 during the event is compared with the imposed model. The difference Δf_{model} (where f_{model} is obtain by averaging the frequency in on 200ms window) is also depicted in Figure 4.14. The values of R^2, obtained for T_w= 200ms, during the selected T_a =10s are depicted in Figure 4.15. The values of CV(RMSE) obtained for T_w= 200ms, during the selected T_a =10s are depicted in Figure 4.16.

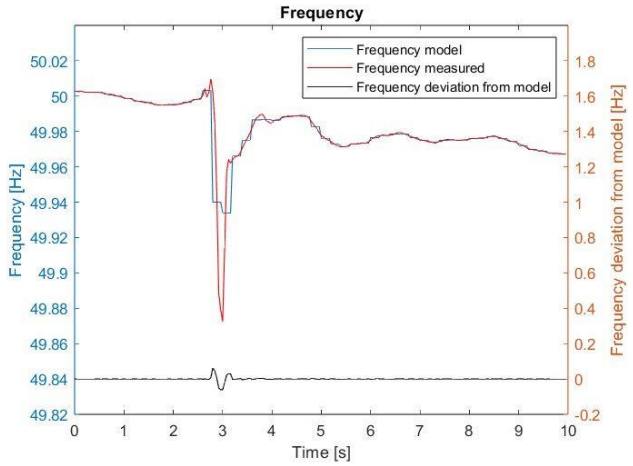

Figure 4.14 Frequency in N_2 during the event on T_{PMU}= 40 ms, T_w= 200 ms, T_a=10 s analysis window, time counted from t_1=313.64 s

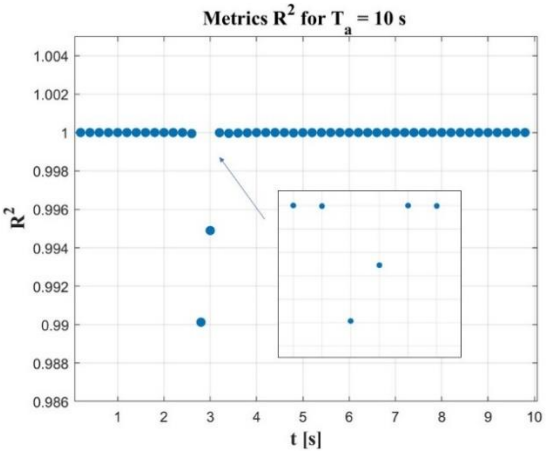

Figure 4.15 R^2values calculated for the frequency signal during the event T_{PMU}= 40 ms, T_w= 200 ms, T_a= 10 s, time counted from t_1=313.64 s

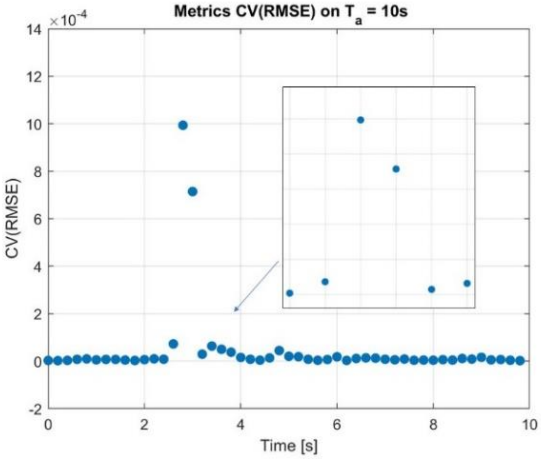

Figure 4.16 CV(RMSE) values calculated for the frequency signal during the event T_{PMU}= 40 ms, T_w= 200 ms, T_a= 10 s, time counted from t_1=313.64 s

Now we analyze the discrepancy between the measured frequency and the steady state model assumed for the power grid. To this, we use a frequency flag: δ. When the frequency deviation from the model exceeds a specified limit $\Delta f_{model,max} = \varepsilon_{max} \cdot f_n$, the flag is raised. The flag takes values 0 (we are within the established limits) or 1 (the imposed limit has been exceeded). The number of flag values is equal to the number of measurements windows T_w in the analysis window T_a.

Figure 4.17 shows the flag δ for the frequency signal during the event, calculated for T_{PMU}= 40 ms, T_w= 1 s, T_a= 10 s, $\Delta f_{model,max} = 0.01$ Hz. One can noticed only two instances where the flag is signalizing deviation from the steady state model. If the measurement window is 200 milliseconds the flag δ we allowed a better localisation of the event as we can see in Figure 4.18.

One can see that the maximum value of CV(RMSE) during the event among the considered 4 nodes is in N_2. Situated on the outskirts of the ENTSO-E system, the N_2 corresponds to the Nuclear Power Plant (CNPP) which comprises of two power generation units, each heaving a capacity of 700 MW. Under certain operational scenarios, the CNPP contributes up to 40% of the overall mechanical inertia in the Romanian Power System. The inertia constant per unit for a nuclear facility at CNPP is 7.29 MW·s/MVA. The proposed metrics can also highlight the inertial steady-state behavior in various nodes of the power system based on the analysis of frequency variation with using an appropriate measurement time.

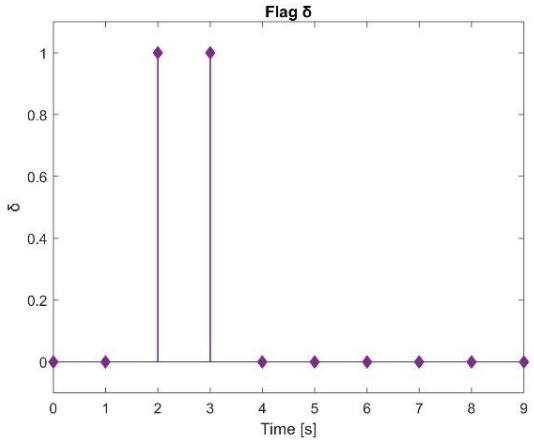

Figure 4.17 The flag δ for the frequency signal during the event, calculated for T_{PMU}= 40 ms, T_w= 1 s, T_a= 10 s, $\Delta f_{model,max} = 0.01$ Hz, time counted from t_1=313.64 s

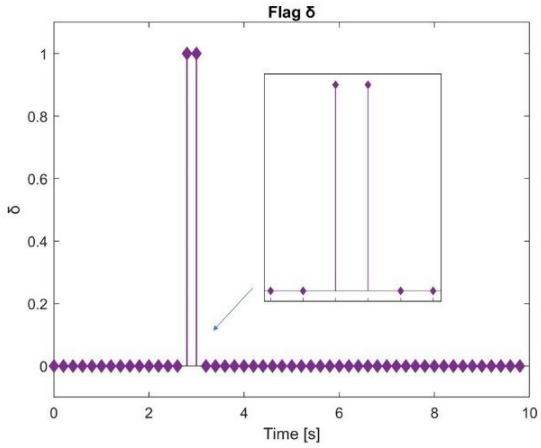

Figure 4.18 The flag δ for the frequency signal during the event, calculated for T_{PMU}= 40 ms, T_w= 200 ms, T_a= 10 s, $\Delta f_{model,max} = 0.01$ Hz, time counted from t_1=313.64 s

Considering all the studies conducted, for specific conditions, we find that CV(RMSD) is a more suitable metric for evaluating frequency variability, using the system's nominal frequency as the reporting value.

In this case for $\bar{y}_p$ in (2.16) we used the system nominal frequency:

$$y_i^* = \frac{\sum_{i=1}^{N_w} f_i}{N_w}; \bar{y}_p = f_n = 50\ Hz \tag{4.7}$$

The results for CV(RMSD) applied to the frequency in N_2 using the assumed model y_i^*, across different temporal reporting windows, are presented in Table 4.13. It can be observed that the highest variability occurs for i=1593, with a value of 0.9%

Table 4.12 Metrics on frequency signal during the event in N_2 for T_w= 200 ms

i	1	2	...	1593	...	3000
CV(RMSD)[%]	0.003	0.003	...	0.897	...	0.002

5 Active power variability

Enhancement in the operation and planning tools for the analysis of active LV distribution grids is a very dynamic field of research [25], motivated by very ambitious targets for greening our society, as stated in the European Green Deal [26]. Analysis tools for cost-efficient, reliable, and safe operation of LV active distribution grids, microgrids and energy communities use as input characteristic power profiles. Analysis of operations and of planning of low voltage (LV) distribution power grids, including their versions for microgrids and energy communities, assume specific power profiles for the loads (individual or aggregated) and for the locally installed power generation (most often photovoltaics). A typical practice is to approximate the power profiles of end-users in the form of energy-related profiles based on aggregated measurements recorded every one hour or down to 30 or 15 minutes. Those assumptions were reasonable for legacy distribution grids with unidirectional power flow, or for distribution grids with low levels of distributed generation. However, the advancement of measurement infrastructure (e.g., smart meters with higher reporting rates) reveal the variability of the load and net-load profiles. Analysis of such profiles using high reporting rate information [27] shows a high variability of the active power flow in the considered network.

Standard measurements used for power system analysis assume that the system remains in steady-state condition between two consecutive measurements [28]. Thus, when a measurement process starts, the assumption is that the behavior of the system is like a generally known model. To verify if the acquired measurement respects the imposed model, several statistical metrics could be applied to estimate the accuracy level. The perfect match between the expected value from the model perspective and the real measurement reveals that the imposed model is the right one. Any difference between the

expected value from the assumed model and the measured once can be statistically assessed to provide an insight on the quality of the imposed measurement model. In the following, an analytical framework that can be used to assess the quality of the assumed power profiles in active distribution grids is proposed. The framework is based on well-known statistical metrics that are selected based on the preliminary requirements of the application (analysis and operation of active LV distribution grids, microgrids and community grids). Furthermore, the proposed methodology considers the availability of information coming from high reporting rate advanced smart meters and IoT technology. We use smart meters, as shown in Figure 5.1, with high reporting rates and make these available to the research community as open data.

Figure 5.1 SMX Landis Gyr

Active power profiles can be used to analyze energy "consumption" or electricity production over a specific period and can provide valuable insights into energy or power usage patterns in a given context. This information is useful in fields such as electrical engineering, energy management, and resource planning. There is a wide variety of consumption profiles depending on the type of consumer: residential power profile (see Figure 5.2), commercial power profile (see Figure 5.3), industrial power profile (see Figures 5.4 and 5.5), and transportation power profile.

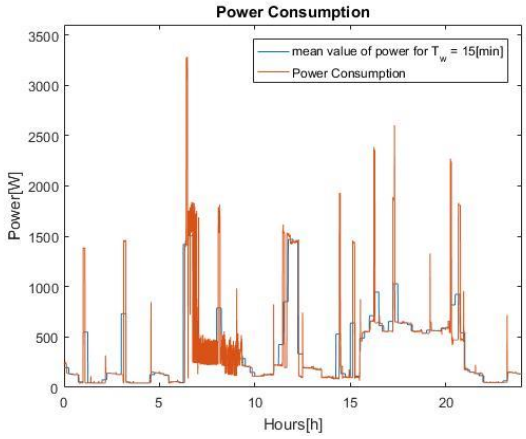

Figure 5.2 Daily load power profile, residential user

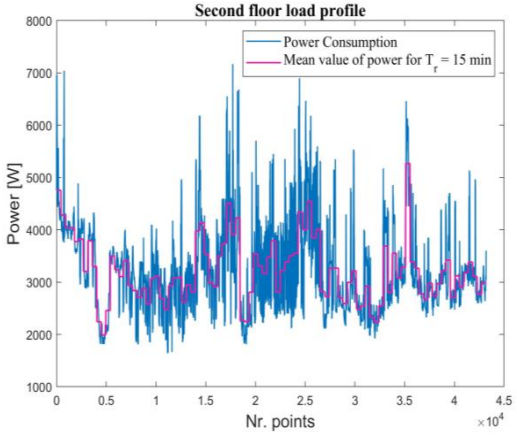

Figure 5.3 Daily load power profile, commercial user

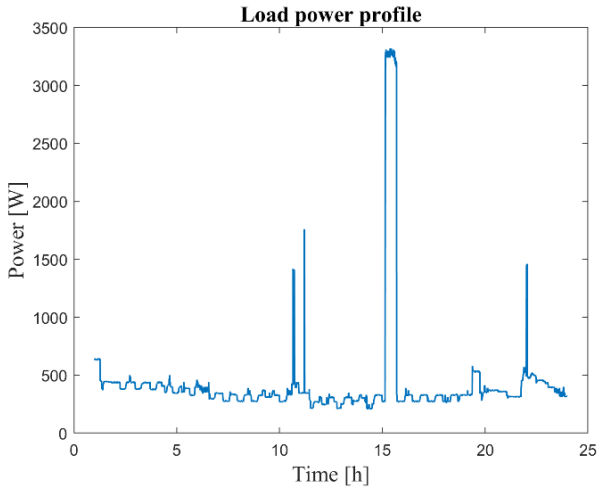

Figure 5.4 Daily load power profile, industrial user

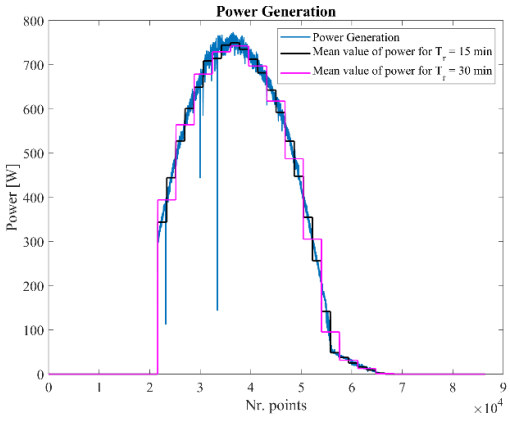

Figure 5.5 Daily generation power profile

5.1 Measurement concept

The information layer used in this study is provided by measurements using the concept of the Unbundled Smart Meter (USM) [29], set on 1 frame/s reporting rate. The USM is an assembly of two parts, the Smart Metrology Meter (SMM) and the Smart Meter eXtension (SMX). SMM is the measurement part (metrology-compliant) providing the measurements, and the SMX, an extension configurable with flexible features to extract, process and stream the instrumentation values from the SMM [30]. The assumption derived from the measurements with low reporting rate is that the measured quantity describes a stationary process so that (i) it remains constant during reporting moments or (ii) the signal model is known and unique during the measurement time (T_w) and during the further aggregation time interval (T_a), if any. The reporting rate in this case is $1/T_a$. In the following, standard signal models describing the energy transfer in LV distribution grids are considered and variability metrics based on T_w, T_a, and f_s, (the sampling frequency used by the respective digital measurement system) are defined. Signal samples need to be available for metrics computation, i.e., the hypothesis that, at least for the duration equal to T_a, all acquired samples are stored by the measurement system and can be used for both the signal model reconstruction and the computation of proposed indicators. Several aggregation windows are considered and two sample rates for the acquired signals are used to illustrate the method. The effect of pre-processing techniques (filtering) in the measurement chain have been neglected at this stage, and the acquired signal is supposed to reflect the energy transfer in the analyzed part of the grid.

The two reporting rates ($T_r = 1/RR$) selected for the purpose of this study are T_r=15 minutes and T_r=30 minutes during which the model (y_i) is represented by a constant power profile: y_i=mean(x_i) while the estimated model (for R^2 computation) is corresponding to a 2 h-constant power profile (T_a=2 h) or to a T_a larger than 2 h (for example, daily):

$$x_i = P_i;\ y_i = \bar{y} = \frac{\sum_{i=1}^{N_r} P_i}{N_r};\ \tilde{y}_i = \frac{\sum_{i=1}^{N_{ss}} P_i}{N_{ss}} = \tilde{y} \tag{5.1}$$

To avoid division by zero, $|y_i - \tilde{y}_i|$ was rounded with Δx_{max}, value chosen suitable for the measurement system:

$$|y_i - \tilde{y}_i| = (|y_i - \tilde{y}_i|, \Delta x_{max}) \tag{5.2}$$

If $y_i - \tilde{y}_i < (\Delta x)_{max,i}$, then $y_i - \tilde{y}_i = (\Delta x)_{max,i} = (\Delta x)_{max} = \varepsilon \cdot P_n$, where ε – absolute error, P_n – nominal active power. Parameters used for a 15 minute window analyzed are T_r= 15 minutes, T_a=2 h, T_{ss}=24 h, N_r=T_r/f_s =900; N_a=N_a= T_a/f_s =7200; N_{ss}=$T_a/f_s = 86400$. Similarly, parameters used for a 30 minutes window analyzed are T_r= 30 minutes, T_a=2 h, T_{ss}=24 h, N_r=T_r/f_s =1800; N_a=N_a= T_a/f_s =7200; N_{ss}=$T_a/f_s = 86400$.

To gain a deeper comprehension of the sequence T_w and T_a in relation to the acquired signal x and to calculate different metrics that assess the deviation from the assumed model y, an illustrative example is depicted in Figure 5.6.

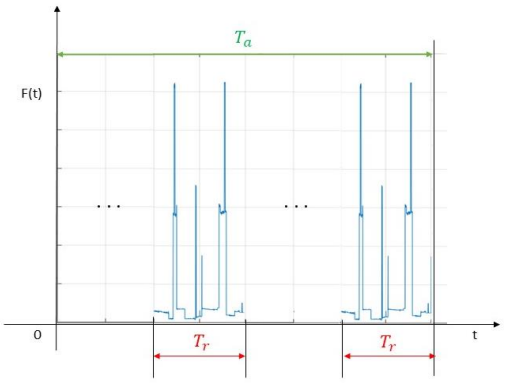

Figure 5.6 Example of time intervals succession

5.2 Correlations between active loads power profiles

We analyzed the load power profile correlation between 2 floors of a student dorm located in the university campus. The time measurement for this study is T_w=1 s and the reporting rate, T_r is 15 minutes. The daily power profile for one floor is presented in blue in Figure 5.7.

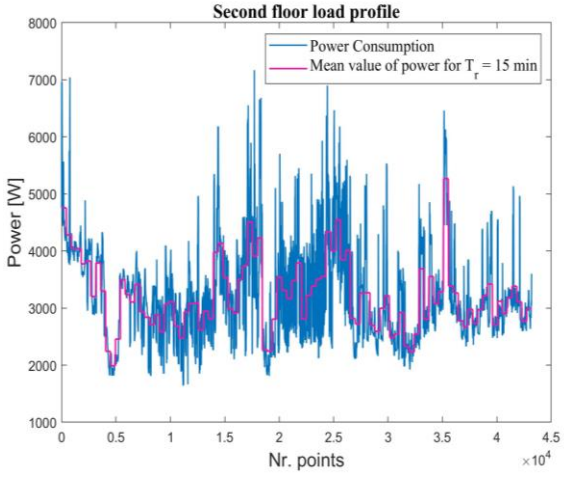

Figure 5.7 Power profile 1 day 2nd floor

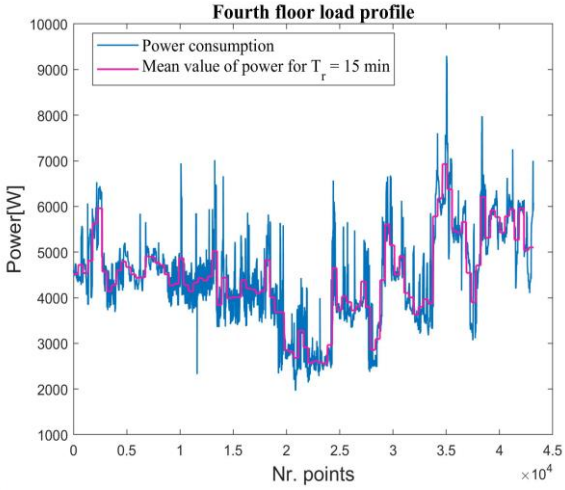

Figure 5.8 Power profile 1day 4th floor

Figure 5.8 presents the load power profile for the fourth floor of the student dorm with blue and with magenta line the mean value made on 15 minutes reporting rate windows. We study the cross correlation between the two power profiles to verify if the two loads have similar behavior as one might expect if students randomly selected from all fields of engineering studies and years of study are living in these dorms. It is to be noted that the latter is a common assumption for power profiling.

In Figure 5.9 the cross correlation between the load profiles for the two floors in the student building is presented. With red are the cross-correlation samples and with blue the bounds (the upper and lower confidence bounds), which are the horizontal lines in the xcf (cross-correlation function) plot. The input data for the cross-correlation matrix is X= $[x_1\ x_2]$, where: $x_1 = P_i = x_i$; (real value); $x_2 = \frac{\sum_{i=1}^{N_r} P_i}{N_r} = y_i = \bar{y}$; (estimated value); C is the resulting correlation coefficient matrix, as presented in Table I, where C (i, j) represents the correlation coefficient between the i-th and j-th variables.

Evaluating the results, the conclusion is drawn that the load power profiles of the two floors are not correlated, due to the value of the cross-correlation function averaging 0.04 for the two separate floors.

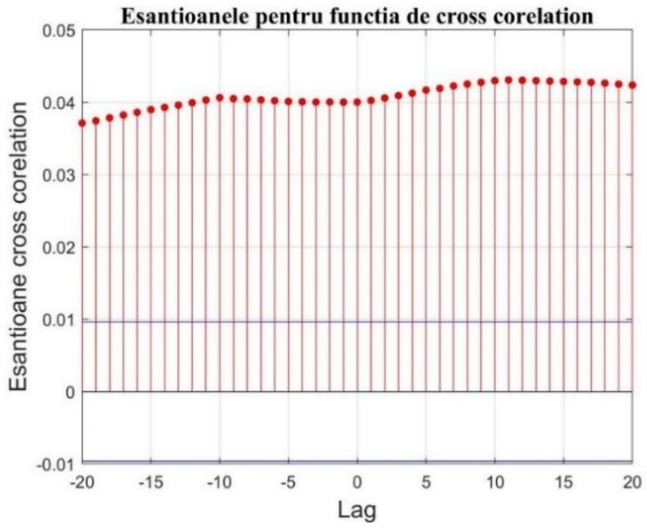

Figure 5.9 Cross correlation between power profiles for 2nd floor and 4th floor consumption

5.3 Active power profile assessment

5.3.1 Case A

To analyze the power profile variability for a household in Bucharest [11], we applied the CV(RMSE) and R^2 metrics for a daily profile available with 1 frame/s reporting rate (f_s=1 sample/s) as depicted in Figure 5.6. The measurement window has been selected T_w=15 minute, during which the model (y_i) is represented by a constant power profile: y_i=mean(x_i) while the estimated model (for R^2 computation) is corresponding to a 2 h-constant power profile (T_a=2 h) or to a T_a larger than 2 h (for example, daily – Figure 5.10).

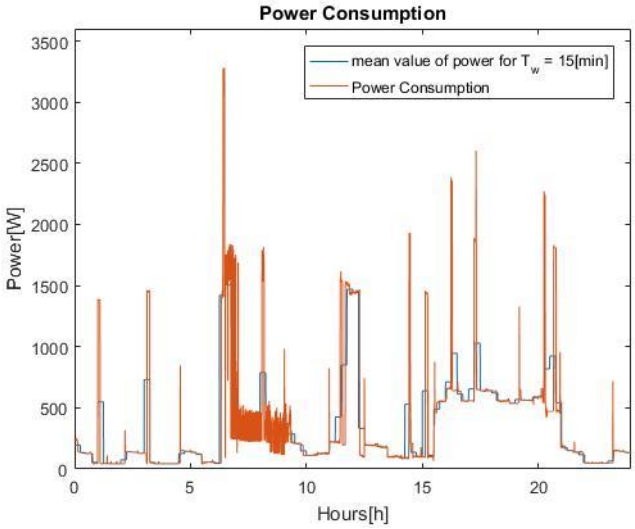

Figure 5.10 The actual power profile ($x[n]$ –red) and the 15-minute average power model($y[n]$ – blue) for a household in Bucharest

Table 5.1 presents the results obtained after applying the two selected metrics for the active power recorded during one day with high reporting rate (1 frame/s). Results represent R^2 maximum over each two hours from a day.

One can observe that we have negative results for the R^2 metric, even though in statistics, the results for this metric are positive for cases where we evaluate a nonlinear function. In such cases, values between -∞ and +∞ can be obtained.

Table 5.1 R^2 and CV(RMSE) for active power on 24 h

Ora	**Timp [min]**	**R^2**	**CV(RMSE)**
00:00-02:00	0-15	-177.91	0.09
	...	...	...
	105-120	0.049	0.005
Min		-33774.28	0.004
Max		0.68	1.31
…			
22:00-24:00	0-1	0.87	0.002
	...	...	...
	105-120	0.81	0.003
Min		-153.38	0.002
Max		0.91	0.08

5.3.2 Case B

To observe the variability of the power profile, we repeat the test with a different dataset, using two reporting rates of 15 minutes and 30 minutes. This time, we perform calculations across a broader range of metrics to assess their suitability for these datasets. The measurement time for this study is T_w=1 s.

Figure 5.11 presents the active power on one day acquired data with 1 s reporting rate and the average on 15- and 30-minutes aggregation time intervals. While it is expected that certain consumption spikes disappear through aggregation, quantifying their severity and persistence within the aggregation time-window is important for reliable and economic operation of several assets within the LV active distribution grids, microgrids [31]. These tables present each metric's result on every reporting rate window and using it we can select the window with the biggest variability. Due to space constraints and to foster brevity only the first and last values are presented. The window that exhibits the highest variability can be identified.

Comparing the metrics results for the two reporting rates $T_r = 15$ minutes and $T_r = 30$ minutes we can observe that there is a bigger difference between the acquired date and the assumed model when the reporting rate is bigger.

It can also be observed that R^2 has both positive and negative values, which confirms that the power consumption profile does not follow a linear function [7]. Additionally, considering these large variations from positive to negative, we conclude that the R^2 metric is not suitable for evaluating the variability of active power. To assess the variability of active power, we consider CV(RMSE) to be a suitable metric.

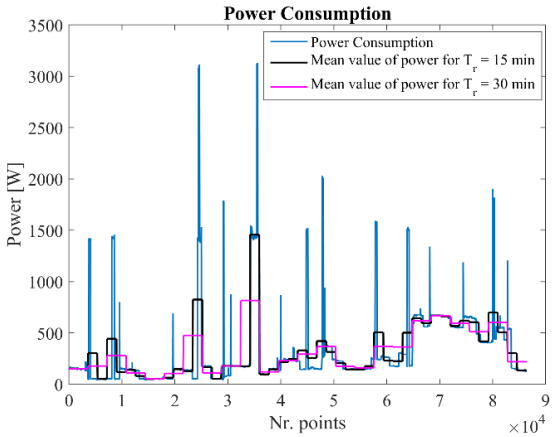

Figure 5.11 The actual power profile and the 15-minute and 30-minutes average power model for a household in Bucharest

Table 5.2 Metrics for active power profile for T_r= 15 - minutes

Nr.	MAE	MSE	RMSE	CV(RMSE)	MAPE	MSPE	R^2	MASE
T_{w1}	5.09E+00	3.49E+01	5.91E+00	2.62E-02	1.23E-03	1.59E-06	-1.21E+01	3.11E+00
T_{w2}	3.20E+00	2.02E+01	4.49E+00	1.99E-02	1.35E-03	6.55E-07	-6.56E+00	1.96E+00
…	…	…	…	…	…	…	…	…
T_{w95}	3.36E+00	3.24E+01	5.69E+00	1.20E-02	3.96E-04	3.74E-07	-9.25E-01	8.19E-01
T_{w96}	2.39E+00	1.05E+01	3.25E+00	6.83E-03	4.00E-04	1.42E-07	3.75E-01	5.83E-01

Table 5.3 Metrics for active power profile for T_r= 30 - minutes

Nr.	MAE	MSE	RMSE	CV(RMSE)	MAPE	MSPE	R^2	MASE
T_{w1}	4.84E+00	4.40E+01	6.63E+00	4.06E-02	1.98E-03	2.19E-04	-1.55E+01	2.95E+00
T_{w2}	1.20E+01	5.45E+02	2.33E+01	1.43E-01	5.33E-02	5.94E-05	-2.03E+02	2.13E+00
…	…	…	…	…	…	…	…	…
T_{w47}	1.84E+02	3.59E+04	1.90E+02	4.62E-01	1.62E-02	4.60E-04	-2.13E+03	3.52E+00
T_{w48}	5.63E+00	5.06E+01	7.12E+00	1.73E-02	9.99E-04	1.24E-06	-2.01E+00	1.37E+00

5.4 Filtering the active power profiles

For a more accurate assessment of the variability of load power profiles, the measurement information was filtered using an adjusted Hampel filter using 2 percentiles p90 and p95 [32]. This process translates into keeping the most probable values of active power for a daily prosumer operation. The decision to implement filtering was made with the aim of establishing a general method for prosumers by removing any anomalies present in their power profiles. The same approach was followed for the other days in July, to discriminate between process variability and pattern anomalies in the daily power profiles.

We apply formula (2.12) and calculate the CV(RMSD) metric on the recorded power profile, the filtered power profile (p90), the filtered power profile (p95), x_i, and the assumed model $y_i = mean(x_i)$ over the window T_r , using the normalized measure $\overline{y_p} = mean(y_i)$ over the window T_a.

Table 5.4 presents the results for the four days by calculating the maximum, mean, and median of CV(RMSD) applied over the duration T_r =1 h.

Table 5.4 CV(RMSD) values for all studied cases

		Recorded power profile	Filtered (p90) power profile	Filtered (p95) power profile
CV (RMSD) 21 July	max	127.0%	14.0%	22.0%
	media	23.0%	9.5%	10.4%
	median	9.7%	9.5%	9.7%
...			...	...
CV (RMSD) 24 July	max	134.0%	75.0%	134.0%
	media	34.0%	20.0%	38.6%
	median	15.2%	13.9%	15.2%

5.5 Active Power Profile for PV installation

The power profile variability for a PV system for the two reporting rates ($T_r = 1/RR$) - 15 minutes and 30 minutes are analyzed in this paragraph. The time measurement for this study is T_w=1 s. Results are compared with the ones obtained for the load curve. Figure 5.12 presents the active power profile for one day acquired data.

Also, Table 5.5 and Table 5.6 present the values for the metrics applied on the active power acquired signal using the two reporting rates. for a daytime interval. These metrics' results provide valuable information about the power system variability, and the table values expose the moment of the day with the biggest difference between the acquired data and the assumed model. By comparing the metrics results for the two reporting rates, $T_r = 15$ minutes and $T_r = 30$ minutes we can notice a more significant disparity between the acquired data and the assumed model when using a larger reporting rate.

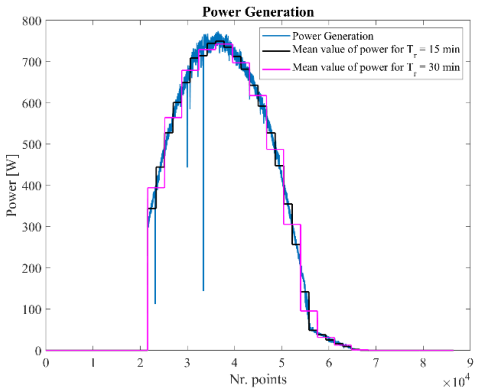

Figure 5.12 The actual power profile and the 15- and 30-minutes, respectively average power model for a PV

Table 5.5 Metrics for active power profile on T_r= 15 - minutes for PV

Nr.	MAE	MSE	RMSE	CV(RMSE)	MAPE	MSPE	R^2	MASE
T_{w1}	5.55E-17	3.08E-33	5.55E-17	3.20E-16	3.56E-17	2.00E-34	1.00E+00	3.20E-14
T_{w2}	5.55E-17	3.08E-33	5.55E-17	3.20E-16	1.78E-17	1.00E-34	1.00E+00	3.20E-14
…	…	…	…	…	…	…	…	…
T_{w95}	3.39E-02	1.81E-03	4.25E-02	2.57E-01	7.77E-03	1.61E-02	-6.60E+02	2.76E+00
T_{w96}	3.42E-02	2.38E-03	4.87E-02	2.95E-01	4.94E-03	4.51E-05	-8.69E+02	2.21E+00

Table 5.6 Metrics for active power profile on T_r= 30 – minutes for PV

Nr.	MAE	MSE	RMSE	CV(RMSE)	MAPE	MSPE	R^2	MASE
T_{w1}	1.22E-15	1.49E-30	1.22E-15	7.04E-15	3.91E-16	9.69E-32	1.00E+00	7.04E-13
…	…	…	…	…	…	…	…	…
T_{w16}	1.90E+01	5.22E+02	2.28E+01	4.67E-02	1.34E-03	1.25E-06	6.33E-01	3.93E-01
…	…	…	…	…	…	…	…	…
T_{w48}	3.39E-02	2.10E-03	4.58E-02	2.77E-01	5.11E-03	1.47E-02	-7.68E+02	2.45E+00

5.6 Net power profile assessment

In the following, we apply the CV(RMSD) metric for three-time intervals over which the assumed model is “constant power profile”, i.e. the reporting rates are: 4 frames/h, 2 frames/h and 1 frames/h. The net power profile is acquired in a microgrid (see Figure 5.13) and P_{net} (Figure 5.16) is computed by the difference between the PV power profile P_{PV} (Figure 5.15) and the load power profile P_l (Figure 5.14).

The data for load- and PV power profiles are acquired synchronously (relative to the measurement frequency, one sample/s).

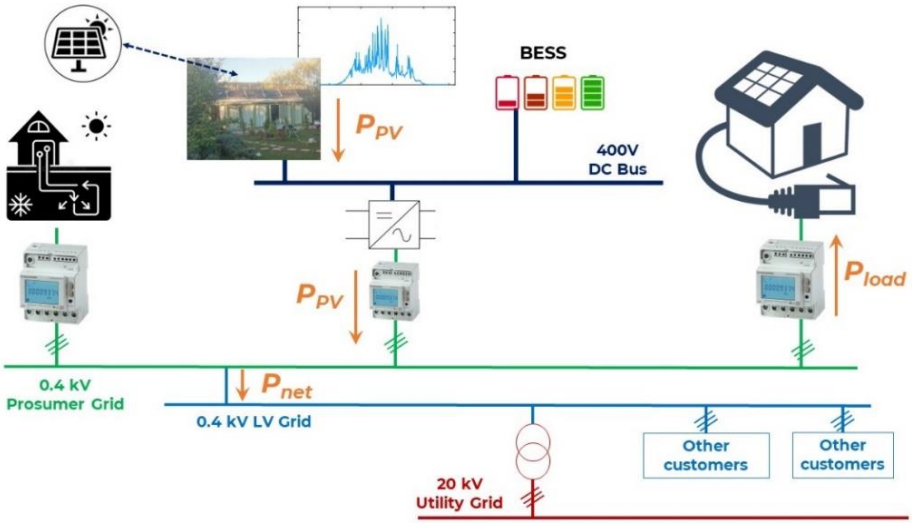

Figure 5.13 Prosumer grid topology

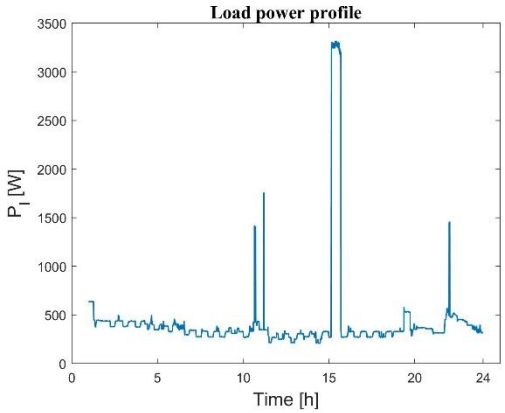

Figure 5.14 Load power profile P_l, on 21 July 2023

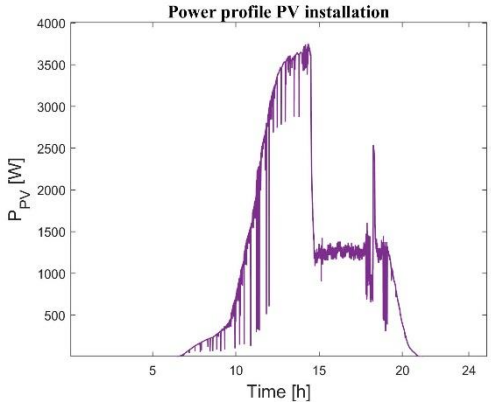

Figure 5.15 Active power profile for a PV, P_{PV}, on 21 July 2023

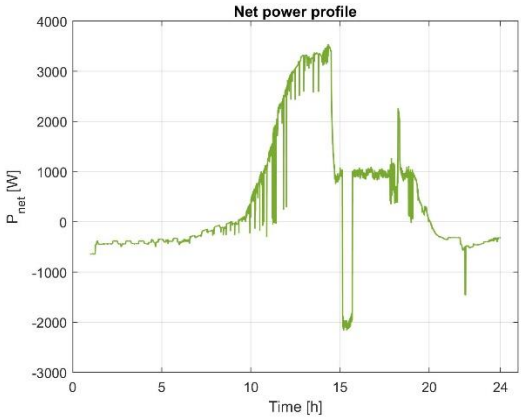

Figure 5.16 Net power profile, P_{net}, on 21 July 2023

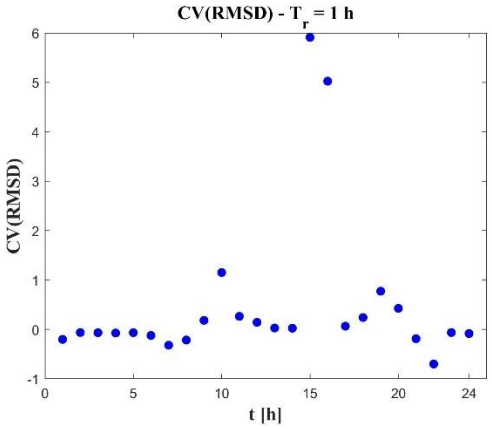

Figure 5.17 CV(RMSD) values for P_{net}, 21 July 2023, T_r = 1h

Figure 5.17 shows the values of the CV(RMSD) metric in the analysis of the 24 hours net power profile, using a reporting rate of 1 hour. It can be observed that the maximum value is 5.9, occurring at 3:00 am, corresponding to T_{r15}.

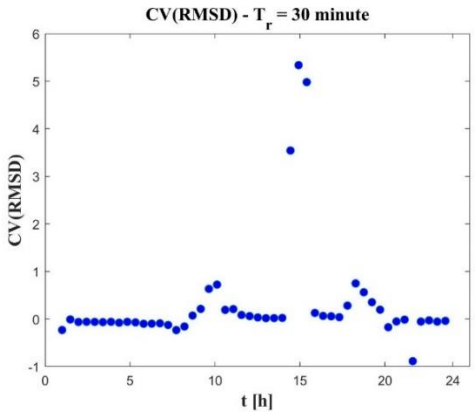

Figure 5.18 CV(RMSD) values for P_{net}, 21 July 2023, T_r = 30 minutes

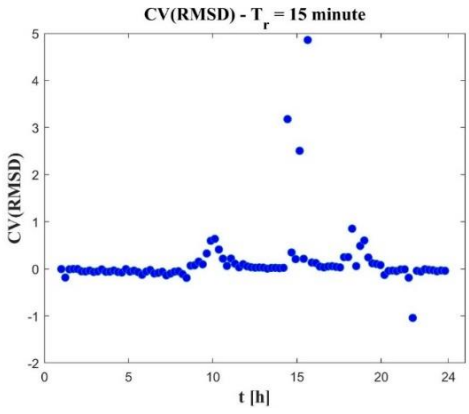

Figure 5.19 CV(RMSD) values for P_{net}, 21 July 2023, T_r = 15 minutes

Figure 5.18 presents the values of the CV(RMSD) metric resulting from the analysis of a 24-hour net power profile, using a reporting rate of 30 minutes. It can be observed that the maximum value is 5.3 at 3:00 pm, corresponding to the T_{r30}. Figure 5.19 shows the values of the CV(RMSD) metric from the analysis of the 24-hour net power profile, using a reporting rate of 15 minutes. It can be observed that the maximum value is 4.85 at 3:30 pm, corresponding to T_{r62}.

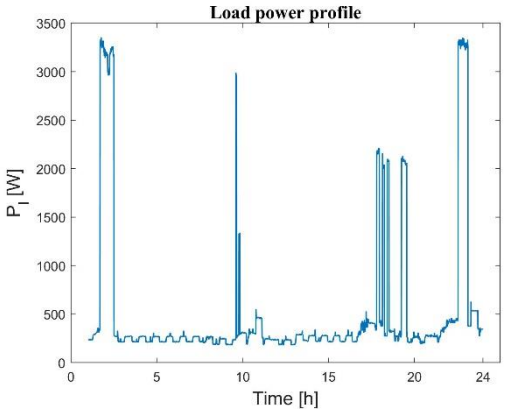

Figure 5.20 Load power profile P_l, on 23 July 2023

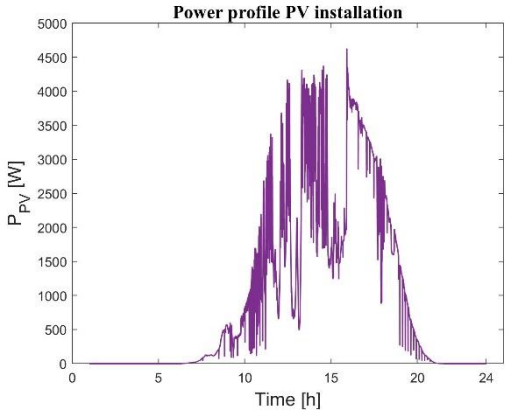

Figure 5.21 Active power profile for a PV, P_{PV}, on 23 July 2023

We repeat the process for a weekend day, July 23, 2023, to observe how the net power profile evolves. Figure 5.22 shows the net power profile, P_{net}, which is obtained by subtracting the load power profile P_l from Figure 5.20 and the photovoltaic system power profile P_{PV} from Figure 5.21. The data on active power consumed and power generated by the photovoltaic panels are collected simultaneously.

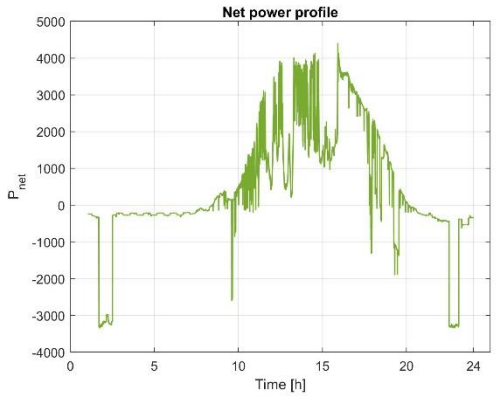

Figure 5.22 Net power profile, P_{net}, in 23 July 2023

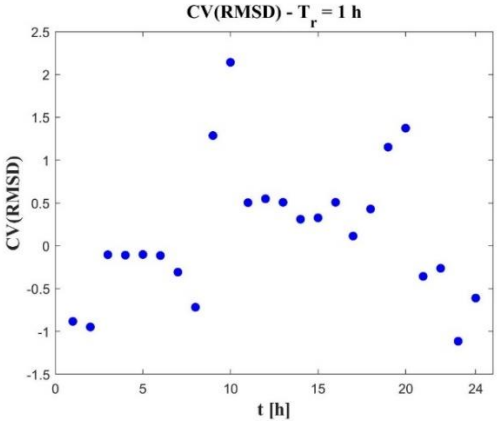

Figure 5.23 CV(RMSD) values for P_{net}, 23 July 2023, T_r = 1h

Figure 5.23 shows the values of the CV(RMSD) metric in the analysis of the 24-hour net power profile, using a reporting rate of 1 hour. It can be observed that the maximum value is 2.14, occurring at 10:00 am, corresponding to T_{r10}. Figure 5.24 presents the values of the CV(RMSD) metric resulting from the analysis of a 24-hour net power profile, using a reporting rate of 30 minutes. It can be observed that the maximum value is 2.4 at 9:30 am, corresponding to T_{r19}. Figure 5.25 shows the values of the CV(RMSD) metric from the analysis of the 24-hour net power profile, using a reporting rate of 15 minutes. It can be observed that the maximum value is 2.87 at 9:15 am, corresponding to T_{r37}

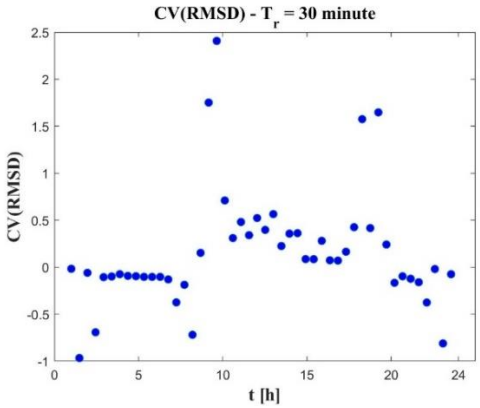

Figure 5.24 CV(RMSD) values for P_{net}, T_r = 30 minutes

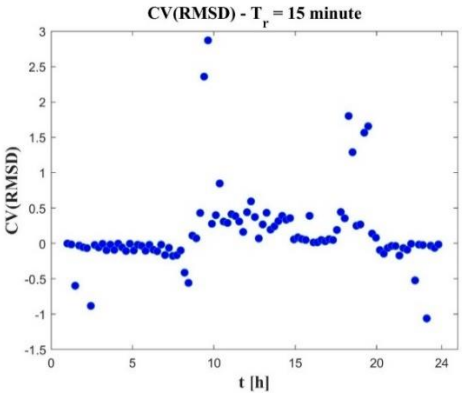

Figure 5.25 CV(RMSD) values for P_{net}, T_r = 15 minutes

To decide how high is the variability in the microgrid, we propose to analyze the median value of the CV(RMSD) for the three signals: load-, PV- and absolute net power profile.

We applied the metric CV(RMSD) on the load power profile, active power profile from the PV installation and absolute net power profile data using different time reporting windows, for two days 21.07.2023 and 23.07.2023, and results for the median values are presented in Table 5.7. It can be observed that the power variability (in terms of CV(RMSD)) is higher for the weekend day 23 July 2023, having the maximum values of 43% for $|P_{net}|$, 15% for P_l and 25% for P_{PV} when T_r = 1 h.

Table 5.7 CV(RMSD) median values

T_r	21.07.2023	23.07.2023	21.07.2023	23.07.2023	21.07.2023	23.07.2023
	CV(RMSD) [%] for $\|P_{net}\|$		CV(RMSD) [%] for P_l		CV(RMSD) [%] for P_{PV}	
1 h	16	43	9	15	6	25
30 min	8	16	8	10	3	7
15 min	6	9	6	6	2	5

However, for specific loading conditions and/or weather (clouds) – depending on power generation, the use of absolute net power profile is hiding the two processes variability and by such is hindering the effectiveness of power control algorithms. Therefore, the CV(RMSD) applied to the net power profile (instead of absolute power profile) appears to be more appropriate.

In this case we use for $\bar{y}_p$ in (2.16) the nominal power of the PV installation:

$$y_i^* = \frac{\sum_{i=1}^{N_r} P_i}{N_r}; \bar{y}_p = P_n = 5\ kW \tag{5.3}$$

Results for CV(RMSD) applied over the net power profile P_{net} on 21.07.2023 using the assumed model y_i^*, on different time reporting windows, are presented in Table 5.8. In can be observed that the maximum depicted values are approximately 30% when the median value is approximately 1%.

Table 5.8 CV(RMSD) values for net power profile

T_r	CV(RMSD) [%]		
	min	**max**	**median**
1 h	0.50	33	1.5
30 min	0.08	30	0.9
15 min	0.02	27	0.7

One can observe that the median CV(RMSD) of the same day 21.07.2023 is significantly lower when using net power profile - with equation (5.3) - than when using absolute power profile (Table 5.7).

We repeat the procedure for one week in June 2023 (17.06.2023 to 23.06.2023) using to observe the net power profile variability. Results for CV(RMSD) applied over P_{net} using the assumed model y_i^*, on time reporting window T_r = 15 minutes, are presented in Table 5.9.

Table 5.9 CV(RMSD) values on net power profiles for one week

Zi	CV(RMSD) [%]		
	min	**median**	**max**
17.06.2023	0.00	0.72	34.43
...	...	...	...
23.06.2023	0.02	1.38	30.56

One can observe that the maximum CV(RMSD) value is 34.43 % on 17 June 2023, the minimum value is 0 for half of the week (recall that a value of 0 signifies an ideal alignment between the model and reality). The median CV(RMSD) value is around 1% for the studied week.

5.7 Information uncertainty

We are exploring a framework for assessing a new model for lack of knowledge associated with the results of a measurement process for parameters characterizing energy transfer that are variable over the measurement and reporting intervals. The concept of information uncertainty, u_{info} is defined as a function of the model variability assessed using the CV(RMSD) statistical metric (computed over a selected interval T_r while in our work we explored T_r as the legacy reporting time of smart meters) and the measurement uncertainty metrologically ensured by the deployed measurement equipment (which is providing measurement information with the reporting rate T_r). We can formulate this relation as:

$$u_{info} = f(T_m, T_r) \tag{5.4}$$

The relationship in (5.4) is based on the time interval T_r that varies depending on the application and assumed model and it is one of the parameters in computed CV(RMSD) and T_m, the sampling period for the measurand data series, provided by an additional measurement system. Thus, giving the formulation of:

$$u_{info} = \sqrt{u_{model}^2 + u_{meas}^2} \tag{5.5}$$

In equation (5.5), u_{model} is the model variability assess using the statistical metric CV(RMSD) and u_{meas} is the classic measurement uncertainty associated with the measurement system. If $T_m = T_r$ then $u_{info} = u_{meas}$. For the case of energy and power measurements, we have used the same meter for acquiring the power samples ($T_m = 1$ s) using the USM technology to access the instrumentation values. For the analyzed example, we can conclude that, using energy measurement values provided with an accuracy class 1 by a smart meter set on hourly reporting rate, the power profile uncertainty during the week in July 2023 is roughly between 10 % and 50 % (median) or, for the filtered (p90) data, between 9 % and 14 %.

6 Application for active power assessment

Measurement information is provided at a high reporting rate using the concept of the Unbundled Smart Meter (USM) [33]. The evaluation of the variability in the electric energy transfer phenomenon can be performed using the CV(RMSD) metric, which was previously presented and studied. To observe the system's variability in real-time based on CV(RMSD), a web application was developed, referred to as PIV (Indicator of Power Variability). The data extracted by Raspberry Pi (RPi) 3 [34] is further processed using this application. Figure 6.1 illustrates the principle behind this application.

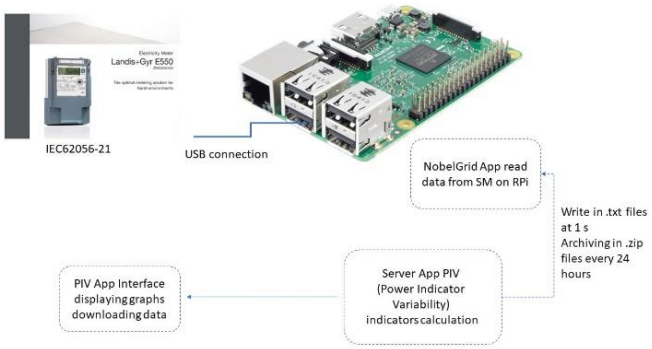

Figure 6.1 Diagram of PIV application

6.1 Logical diagram and software implementation

PIV is an application developed using Python [35] programming language and Flask [36] as the framework for building the web server. The PIV application employs Ngrok [37] to provide a secure access path to the Flask server.

The calculation and data processing logic for the data acquired from the meter was implemented using the Python language. For the calculations, we used the "numpy" library.

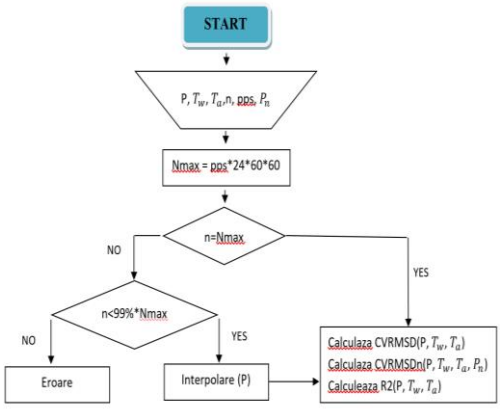

Figure 6.2 Logical diagram of PIV

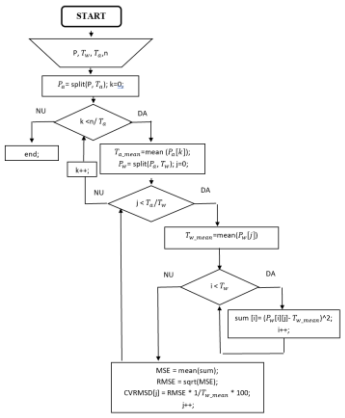

Figure 6.3 Logical diagram of CV(RMSD) function

In Figure 6.2, the operation of the Server App PIV, the back-end part of the PIV application, is presented. It shows that the application receives the following input data: P – active power, T_w- measurement window, T_a- aggregation window, n - number of current record values, pps - number of points per second, P_n- approved active power for the consumer.

Figure 6.2 shows the simplified logical scheme of the application, and the two functions that calculate the metrics are detailed in Figures 6.3, 6.4, and 6.5.

Figure 6.3 presents the logical scheme used for implementing the CV(RMSD) metric calculation. The function takes as input data P, T_w, T_a, and n, and outputs a vector with the CV(RMSD) values. The scheme shows how the data set vector P is decomposed into vectors P_a of the length of the T_a window, and then each P_a vector is further decomposed into P_w vectors of the length T_w. After decomposing the P vector, the creation of the CVRMSD[j] vector begins. The first step is to create a sum[i] vector whose elements are the square of the differences between each P_w element and the mean T_{w_mean}. After obtaining this vector, its mean is calculated, the square root is extracted to obtain the RMSE, and the final step is to divide the RMSE by T_{w_mean} and multiply by 100 to have a percentage representation. Thus, the first element of CVRMSD[j] is created, and the process is repeated until the vector is completed with n/T_w elements.

Figure 6.4 presents the logical scheme used for implementing the calculation of the $CV(RMSD)_n$ metric. It is similar to CV(RMSD), but the final step involves dividing the RMSE by P_n - the nominal power approved for the user and multiplying by 100 to have a percentage representation. Thus, the first element of CVRMSDn[j] is created, and the process is repeated until the vector is completed with n/T_w elements.

Figure 6.5 presents the logical scheme used for implementing the calculation of the R^2metric. The function takes as input data P, T_w, T_a, n, and limit (imposed value) and outputs a vector with the R^2values. The scheme presents a data set decomposition process similar to that of the CV(RMSD) calculation. After decomposing the P vector, the creation of the R2[j] vector begins. A sum[i] vector is created, whose elements are the square of the differences between each P_w element and the mean T_{w_mean}. After obtaining the numerator, the denominator is calculated. The difference diff between $T_{w_mean}$and $T_{a_mean}$is calculated, then it is checked that this is not less than an imposed limit; if true, diff is set to the limit, otherwise, the process continues with diff. The denominator is obtained by squaring the differences and multiplying them by T_w. The first element of R2[j] is obtained by subtracting from 1 the sum of the elements of sum[i] divided by the obtained denominator num_z. The process is repeated until the vector is completed with n/$T_w$elements.

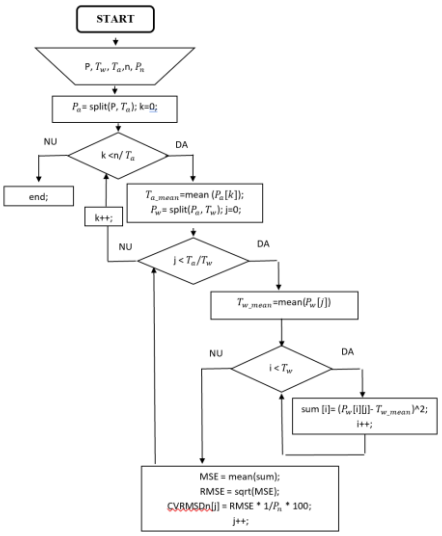

Figure 6.4 Logical diagram of $CV(RMSD)_n$ function

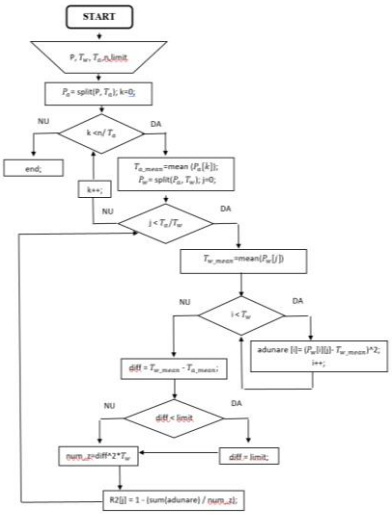

Figure 6.5 Logical diagram of R^2 function

6.2 Data preprocessing

Data preprocessing is a process of preparing and transforming raw data into a suitable form for further analysis, machine learning, or other data processing tasks. This step is essential in the data analysis process and involves several operations, including cleaning, transforming, standardizing, and reducing the dimensionality of the data.

The PIV application performs the following preprocessing operations:

Data cleaning: identifying and correcting errors in the data, such as missing values through interpolation (if a maximum of 1% of the data is missing) and NaN values by replacing them with the mean of the data series.

Standardization and normalization: converting timestamp data from a standardized date format for efficient future use.

Data splitting: dividing the dataset into subsets for processing, timestamp, and power. For missing data replacement, the PIV application uses an interpolation function when less than 1% of the data is missing (e.g., one day of data acquired with SMX, with a reporting rate of 1 frame/s, contains 86,400 values, so the maximum number of missing values would be 864). If more than 1% of the data is missing, the user receives a message indicating the number of recorded data points for that day and that the acquisition was corrupted.

We used linear interpolation to replace missing data because this mathematical technique is employed to estimate values between known points in a data series. It involves constructing a linear function that passes through the known data points and then using this function to estimate the values between these points. Interpolation is often used when we have limited or unevenly distributed data and want to estimate values between these data points.

For replacing missing values x_i, another imputation method could be implemented based on identifying the index "i" of the missing values. Knowing the exact indices for which the values are missing, these could be replaced with the average values over the window T_w or with a nominal value (e.g., the installed power).

6.3 Web interface description

The graphical interface for the PIV application is designed using web technologies such as HTML, CSS, and JavaScript, thus providing an interactive and user-friendly experience. These web technologies enable the creation of a responsive graphical interface, adapted to various screen sizes, including those of mobile devices.

When accessing the web page, an authentication system opens (see Figure 6.6), designed to protect resources. By implementing authentication, access to resources is controlled. We used this system to ensure information security, access control, protection against unauthorized access, and monitoring of user activities.

After entering the authentication details, such as the username and password, the web page opens as shown in Figure 6.7.

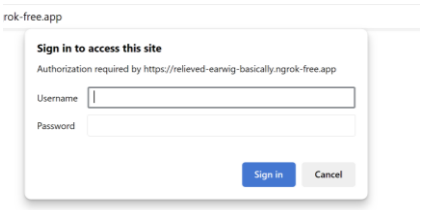

Figure 6.6 Authentication system

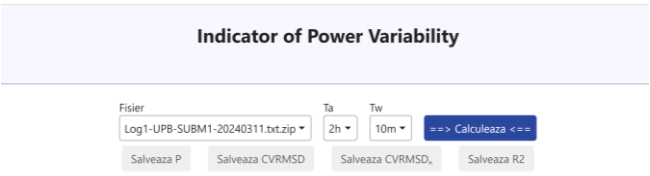

Figure 6.7 PIV web interface

The interface features a file section, represented by a selection box (see Figure 6.8), which allows users to select the input data file they wish to analyze. Files in .zip or .txt formats can be chosen. Users can upload .zip archives containing datasets from previous periods. The .txt format is reserved for data from the current day, but calculations cannot be performed on it because the file is not complete.

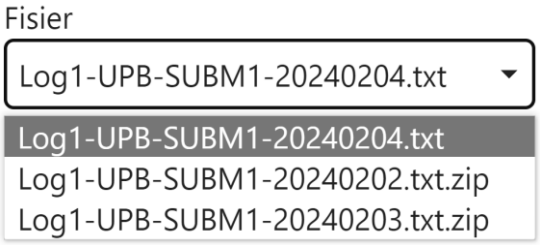

Figure 6.8 Drop down bottom for File selection

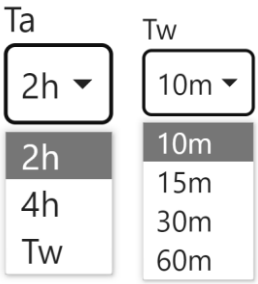

Figure 6.9 Drop down bottom for windows Ta, Tw selection

The user can select the windows for which they want to calculate the CV(RMSD) metric using the Ta and Tw checkboxes. Ta can be set to either 2 hours or 4 hours, while Tw can be set to 10, 15, 30 minutes, or 1 hour (see Figure 6.9).

Clicking the "==> Calculeaza <==" button initiates the calculation process for the CV(RMSD), $CV(RMSD)_n$ and R^2 metrics based on the provided input data and selected windows. The results are displayed in the form of a scatter plot (see Figure 6.10), and additional information about the processed file is provided: acquisition date (e.g., 2024-02-11), reporting rate of the data (e.g., 1 frame/s), and the number of data points acquired (e.g., 86395) out of the total possible number (e.g., 86400), and the approved nominal power for the user P_n (e.g., 2 kW).

In Figure 6.11, we can see how the CV(RMSD) metric results are represented with blue points. Hovering over a point with the mouse provides two pieces of information: the value of the metric and the window T_w for which it was obtained.

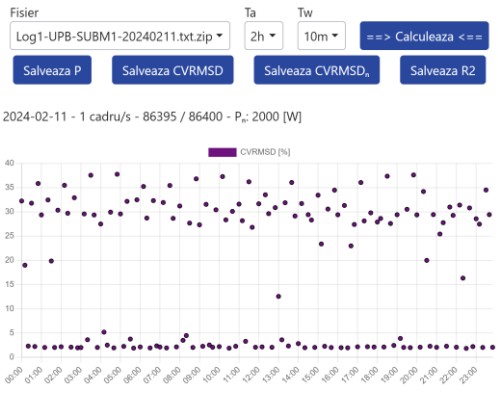

Figure 6.10 CV(RMSD) graph

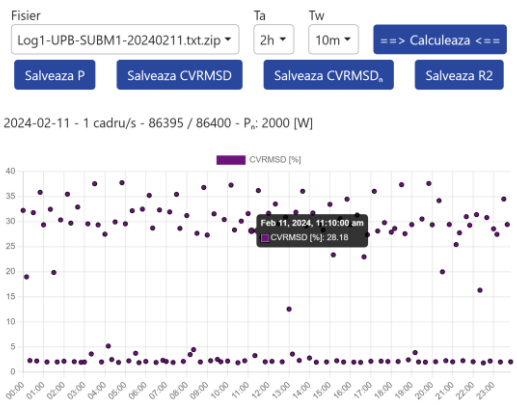

Figure 6.11 Web interface graphics

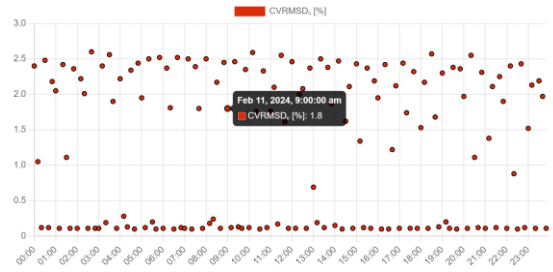

Figure 6.12 $CV(RMSD)_n$ graph

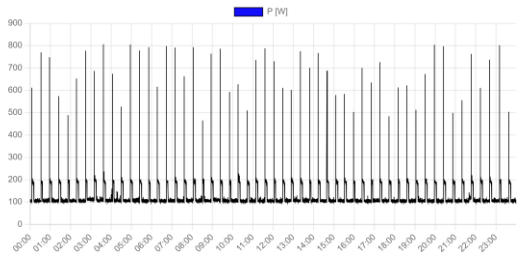

Figure 6.13 Load power profile

In Figure 6.12, the second graph generated by clicking the "==> Calculeaza <==" button shows the results of the $CV(RMSD)_n$.metric.

Figure 6.13 illustrates the third graph generated by clicking the "==> Calculate <==" button, representing the load power profile "P" for a day. This data, acquired using SMX, is used as input for the metric calculations.

The resulting data can be downloaded in .csv format by clicking the three buttons. "Salveaza P" allows downloading the power data used as input for the metric calculations. "Salveaza CVRMSD" downloads the calculated CVRMSD values. "Salveaza R2" downloads the calculated R^2 values.

This provides the ability to store the data for further processing, as shown in Figure 6.14.

Figure 6.14 "Salveaza" buttons

The PIV application ensures a pleasant and intuitive user experience by providing easy and quick access to the CV(RMSD) metric results. The execution time required to compute the final results depends on the processing power of the server hosting the application. Considering the complexity of the calculations, the large volume of data that needs to be processed (1 day of data with a 1 frame/s rate—totaling 86400 frames), the need to display data (3 graphs), and the computing power of the RPi, the estimated execution time of the application is 32 seconds. In this case, the different types of windows T_r do not affect the execution time.

7 Conclusions and personal contributions

7.1 Conclusions

Measurements in the LV grids are performed with a silently assumed model for the phenomena governing the energy transfer.

Among those models, the steady-state operation considers for voltage signals constant rms value, frequency, and phase.

We proposed several indicators and then we selected two of them: coefficient of determination (R^2) and the coefficient of variation of RMSE (CV-RMSE) able to easily quantify the deviation of the signal from the assumed signal model. This metrics are easy to be implemented using the available signal samples and, together with a user-defined level, can trigger a warning signal linked to the measured value. This warning is independent of the measurement quality and captures the potential inadequacy of the assumed model during the time interval required by reporting the measurement values.

For power profiles, even when derived from smart meters measurements, the model is built on constant 15 minutes power values, although measurements with 1s reporting rate show high variability in the energy transfer. Those assumptions are usually extended from the measurement time to the reporting time intervals.

We proposed two metrics for discriminating steady state from dynamic operation of a power system based on frequency measurements: the coefficient of determination (R^2) and the coefficient of variation of RMSE (CV(RMSE)). The two metrics use a measurement window adapted to the available inertia. For Romanian Power System the best localizing effect is obtained for T_w= 200ms when the frequency information is available with T_{PMU}= 40ms. CV(RMSE) offers a better resolution for

identifying events deviation from steady-state operation. In addition, we proposed the use of a flag δ to identify events by comparing the frequency deviation from the assumed model within a specified limit $\Delta f_{model,max}$. In this case the model is proposed as the average frequency signal over T_w. These two metrics, together with the proposed flag, can be used for monitoring the stability in networks with low inertia.

In this paper an analytical framework was introduced aiming for the analysis of highly variable and high reporting rate power profiles in respect to the predefined models. A statistical approach based on describing the matching mathematical problem between two sets of data, one observed/acquired via measurements and one estimated/imposed, based on a pre-defined measurement model, is used to define and study an electrical engineering problem as part of the power quality assessment.

The load power profile cross correlation reveals that the users have different types of consumption even when they have similar schedules and behaviors. Further studies on both generation and consumption profiles reveal the impact of the reporting rate on the suitability of the model.

For the active power profiles, it can also be observed a significant variability in the energy transfer at second level. All these results validate the need to further study the appropriateness of the classical models for both load curves and generation profiles when dealing with the new type of grids like the ones in energy communities. It is also highlighted that the proposed assessment framework could be beneficial for the appropriate selection of characteristic power profiles to be used in several planning and operation applications for analysis of LV distribution grids, microgrids or energy communities.

In this paper we consider a prosumer for which both loading, and generation power profiles are available with a synchronous sample rate of 1 sample/s. The variability has been quantified for two different loading conditions (weekday and weekend day) and three different constant power models (T_r = 1 h, 30 minutes and 15 minutes). To assess the impact of the prosumer on the distribution grid the indicator CV(RMSD) has been calculated for net power profile and absolute power profile. The use of net power profile with a presumed model value selected as a nominal PV generation power proves to be more appropriate for assessing power profiles variability in LV networks.

The CV(RMSD) metric provides a more accurate representation of voltage variation by normalizing the RMS deviation relative to the mean, allowing for a consistent comparison across different scales. Its ability to reveal intricate patterns of network behaviour and assess temporal stability makes it indispensable useful tool for advancing the reliability and performance of power distribution systems. Future work aims at integrating CV(RMSD) into standard monitoring practices and exploring its potential in predictive maintenance algorithms to further enhance power quality management. The proposed metrics, derived from statistical tools, can be considered as topology agnostic. Those are not intended as a replacement for classical methods to evaluate network performance and variability, but they add another dimension to the available information and invite to reconsider the steady state models and their implicit time constants for power flow analysis in emerging, low inertia, networks. The impact of the measurement chain on the results is part of a future endeavor.

The application of PIV guarantees a user-friendly and intuitive experience, facilitating straightforward and rapid access to metric results. This framework is adaptable to various data types and reporting frequencies and can be expanded to process additional metrics. Its flexibility, coupled with the integration of the smart meter extension, renders it a valuable tool for the preliminary analysis of grid nodes. Future research will aim to employ this application as an embedded indicator of power variability within smart meters. Furthermore, the application will be integrated with other smart meters, encompassing those on university campuses, residential settings, and prosumer grids.

7.2 Personal contributions

Evaluation of power system variability using statistical metrics.

A new δ indicator is proposed to monitor stability in networks with low inertia.

A comprehensive set of statistical indicators is provided for quantifying the quality of specific profiles used in the analysis of active LV distribution networks and energy communities.

The impact of prosumers on the distribution network is evaluated using the CV(RMSD) indicator for net power profiles and absolute power profiles. It is demonstrated that using the net power profile with a presumed nominal PV generation power model is more appropriate for evaluating power profile variability in medium-voltage networks.

Variability is assessed based on the effective signal value, applying the coefficient of variation of the root mean square deviation (CV(RMSD)). A key finding of the study is that the measurement system used for effective voltage values affects the quality of information in medium-voltage distribution networks.

The preliminary analysis involves testing conventional statistical metrics on energy system parameters (voltage, frequency, power) and selecting suitable metrics for observing variability in low-voltage electrical networks, with results published in Stud 1, (see ANNEX).

The analysis of frequency variability in networks is highlighted by applying appropriate metrics to signal moments of instability, with results published in Stud 2, (see ANNEX).

This analysis examines the variability of active power by evaluating different consumption profiles from various consumers and generation profiles using statistical metrics, with results published in Stud 3, (see ANNEX).

The variability of the effective voltage value is analyzed using the coefficient of variation of the root mean square deviation (CV(RMSD)), with results published in Stud 4, (see ANNEX).

The analysis of net power profiles for prosumers with photovoltaic panel generation is presented, with results published in Stud 5, (see ANNEX).

A web application integrated with Raspberry Pi (RPi) and meters is developed, capable of evaluating, utilizing, and post-processing the results of metrics CV(RMSD), $\mathrm{CV(RMSD)}_n$ și R^2.

Bibliography

[1] H. Albert, Ș. Gheorghe, N. Golovanov, L. Elefterescu, R. Porumb – "Calitatea energiei electrice Contribuții. Rezultate. Perspective", Editura AGIR, București 2013

[2] A. Baggini, "Handbook of Power Quality", Ltd, 2008, John Wiley & Sons, 2008.

[3] G. Wiczynski, "Analysis of Voltage Fluctuations in Power Networks," in IEEE Transactions on Instrumentation and Measurement, vol. 57, no. 11, pp. 2655-2664, Nov. 2008

[4] M. Calin and A. M. Dumitrescu, "Stationarity hypothesis in power systems data aggregation. Verification algorithm," 2013 8TH INTERNATIONAL SYMPOSIUM ON ADVANCED TOPICS IN ELECTRICAL ENGINEERING (ATEE), Bucharest, Romania, 2013, pp. 1-4

[5] IEC 61000-4-30 ed3.0, Electromagnetic compatibility (EMC) - Part 4-30: Testing and measurement techniques - Power quality measurement methods, 2015.

[6] P. Bharadwaj, J. Agrawal, R. Jaddivada, M. Zhang, M. Ilic – "Measurement-based Validation of Energy-Space Modelling in Multi-Energy Systems", 52nd North American Power Symposium (NAPS) | 978-1-7281-8192-9/21/$31.00 ©2021 IEEE

[7] D. Chicco, M. J. Warrens, G. Jurman - "The coefficient of determination R-squared is more informative than SMAPE, MAE, MAPE, MSE and RMSE in regression analysis evaluation", PeerJ Comput. Sci.

[8] A. Riepnieks, H. Kirkham – "An Introduction to Goodness of Fit for PMU Parameter Estimation", IEEE Transactions on Power Delivery,2016

[9] A. Shapiro, Y. Xie and R. Zhang, "Goodness-of-Fit Tests on Manifolds," in IEEE Transactions on Information Theory, vol. 67, no. 4, pp. 2539-2553, April 2021.

[10] H. Kirkham, R. White and M. Albu, "Dealing with Definitional Uncertainty Better Measurements in Power Systems", 2019 IEEE 10th International Workshop on Applied Measurements for Power Systems (AMPS), 2019, pp. 1-6.

[11] Broșură tehnică: "BlackBox G4500 The 3 Phases Portable Power Quality Analyzers", disponibil la: www.elspec-ltd.com, accesat la 20.04.2021

[12] Broșură tehnică: „Arbiter Systems, Inc., Arbiter1133a Data Sheet", accesat la 20.04.2021

[13] A. Ioanid, D. Palade, "The role of distribution system operators in the decentralized power system", RRST-EE, vol. 69, 1, pp. 33–38, Bucharest, 2024

[14] M. Gavrilaș, R. Toma, "Flexible alternating current transmission system optimization in the context of large disturbance voltage stability", RRST-EE, vol. 66, no. 1, pp. 21–26, Apr. 2021

[15] G. Shahgholian, S. Mohammad Ali Zanjani, “A study of voltage sag in distribution system and evaluation of the effect of wind farm equipped with doubly-fed induction generator”, RRST-EE, vol. 68, 3, pp. 271–276, Bucharest, 2023

[16] D. Macii and D. Petri, "Rapid Voltage Change Detection: Limits of the IEC Standard Approach and Possible Solutions," in IEEE Transactions on Instrumentation and Measurement, vol. 69, no. 2, pp. 382-392, Feb. 2020.

[17] A. R. Toma, A. -M. Dumitrescu and M. Albu, "Impact of measurement set-up on RVC-like event detection," 2016 IEEE International Instrumentation and Measurement Technology Conference Proceedings, Taipei, Taiwan, 2016, pp. 1-5.

[18] A. P. Brîncoveanu, E. Fiorentis, A. -M. Dumitrescu and M. M. Albu, "Signal Model Adequacy Indicator for Measurements in LV Grids," 2023 IEEE International Instrumentation and Measurement Technology Conference (I2MTC), Kuala Lumpur, Malaysia, 2023, pp. 1-6

[19] R. Plamanescu, M. Pitz, M. Maghnie, C. Deaconescu, G. Stamatescu, D. M¨uller, A. Monti, M. Albu – “Open-source platform for integrating high-reporting rate information using FIWARE technology”, 2023 IEEE 13th International Workshop on Applied Measurements for Power Systems (AMPS)

[20] IEC/IEEE 60255-118-1:2018, Measuring relays and protection equipment - Part 118-1: Synchrophasor for power systems – Measurements, 2018

[21] IEEE Guide for Phasor Data Concentrator Requirements for Power System Protection, Control, and Monitoring, IEEE Standard C37.244-2013

[22] MicroDERLab - https://www.microderlab.upb.ro, accesat la 25.02.2024

[23] L. Toma, M. Sanduleac, D. Sidea, C. Stanescu, C. Diaconu, M. Albu, A. Dumitrescu, "Frequency Dynamics in the Romanian Power System under Large Perturbations," 2020 55th International Universities Power Engineering Conference (UPEC), Turin, Italy, 2020, pp. 1-6.

[24] Transelectrica S.A, „Romanian transmision network”- disponibil la - www.transelectrica.ro, accesat la 4.08.2023.

[25] Al-Jaafreh, M. A.A, Mokryani, G. – “Planning and operation of LV distribution networks: a comprehensive review, ” IET Energy Systems Integration, pp. 1-15, July 2019.

[26] Simon, Frédéric, et al. - "EU Commission unveils 'European Green Deal': The key points", Dec. 2019, disponibil la: www.euractiv.com. Retrieved 2023-05-27.

[27] M. Sănduleac, I. Ciornei, et. al., "High Reporting Rate Smart Metering Data for Enhanced Grid Monitoring and Services for Energy Communities, IEEE Transactions on Industrial Informatics, vol. 18, no. 6, pp. 4039-4048, June 2022.

[28] S. Chakrabarti, E. Kyriakides, T. Bi, D. Cai and V. Terzija, "Measurements get together," IEEE Power and Energy Magazine, vol. 7, no. 1, pp. 41-49, Jan.-Feb. 2009.

[29] NOBEL GRID Project, *op. cit.* p. 27

[30] R. Plamanescu, M. V. Olteanu, V. Petre, A. -M. Dumitrescu, M. Albu, „Knowledge Extraction from Highly Variable Power Profiles In University Campus”, U.P.B. Sci. Bull., Series C, Vol. 84, Iss. 4, 2022, ISSN 2286-3540

[31] A. R. Toma, M. V. Olteanu, A. -M. Dumitrescu, Campus Load Profiles from Enhanced Smart Meter Data, 2019 54th International Universities Power Engineering Conference (UPEC), 2019, pg. 1-4.

[32] R. K. Pearson, Y. Neuvo, J. Astola, M. Gabbouj – “Generalized Hampel Filters”, EURASIP J. Adv. Signal Process. 2016, 87 (2016).

[33] M. Sanduleac, L. Pons, G. Fiorentino, R. Pop and M. Albu, "The unbundled smart meter concept in a synchro-SCADA framework," 2016 IEEE International Instrumentation and Measurement Technology Conference Proceedings, Taipei, Taiwan, 2016, pp. 1-5.

[34] Raspberry Pi Foundation, “Raspberry pi 3 model b.” disponibil la: https://www.raspberrypi.com/products/raspberry-pi-3-model-b/, accesat la 10.02.2024.

[35] https://www.python.org/, accesat la 20.11.2023

[36] https://flask.palletsprojects.com/en/3.0.x/, accesat la 20.11.2023

[37] https://ngrok.com/, accesat la 20.11.2023

ANNEX

L I S T
scientific works in the field of doctoral thesis

A. ISI/BDI indexed papers published

1. Stud1: **A. P. Brîncoveanu**, E. Fiorentis, A. -M. Dumitrescu and M. M. Albu, "Signal Model Adequacy Indicator for Measurements in LV Grids," *2023 IEEE International Instrumentation and Measurement Technology Conference (I2MTC)*, Kuala Lumpur, Malaysia, 2023, pp. 1-6, doi: 10.1109/I2MTC53148.2023.10175891.

2. Stud2: **A. P. Brîncoveanu**, E. Fiorentis, A. -M. Dumitrescu, *M. M. Albu*, **2023**, "Assessing Frequency Variability Using Long Term High Reporting Rate Measurements," *2023 International Conference on Electromechanical and Energy Systems (SIELMEN)*, Craiova, Romania, 2023, pp. 1-6, doi: 10.1109/SIELMEN59038.2023.10290822

3. Stud3: **A. P. Brîncoveanu**, R. Plămănescu, A. -M. Dumitrescu, I. Ciornei, **2023**, "Assessment of Power Profiles in LV Distribution Grids," *2023 8th International Symposium on Electrical and Electronics Engineering (ISEEE)*, Galati, Romania, 2023, pp. 69-74, doi: 10.1109/ISEEE58596.2023.10310322

4. Stud6: **A. P. Brîncoveanu**, R. Plămănescu, A. -M. Dumitrescu and M. Albu, "Measurement and Information Uncertainty for Highly Variable Power Profiles," *2024 IEEE International Instrumentation and Measurement Technology Conference (I2MTC)*, Glasgow, United Kingdom, 2024, pp. 1-6, doi: 10.1109/I2MTC60896.2024.10560907.

5. Stud4: A. P. Brîncoveanu, R. Plămănescu, A. -M. Dumitrescu and M. Albu, "Voltage variability assessment in power systems", RRST-EE, vol. 69, no. 2, pp. 171–176, Jul. 2024, doi: 10.59277/RRST-EE.2024.2.9, WOS:001265977200009.

B. ISI/BDI/WOS indexed works in progress

1. Stud5: **A. P. Brîncoveanu**, R. Plămănescu, A. -M. Dumitrescu and M. Albu, "Variability assessment of net power profiles for prosumers with PV generation" U.P.B. Sci. Bull. – under review.
2. Stud7: **A. P. Brîncoveanu**, E. Fiorentis, R. Plămănescu, A. -M. Dumitrescu and M. Albu, "Estimation of the LV power profiles variability using the Goodness of Fit approach", *14th IEEE International Workshop on Applied Measurements for Power Systems (AMPS*), 2024 – accepted to publication.
3. Stud8: **A. P. Brîncoveanu**, A. -M. Dumitrescu, "Embedded application for power flow variability assessment", *The International Conference on Applied and Theoretical Electricity (ICATE 2024)*, 2024 – under review.

C. Other works in progress

1. Stud9: **A. P. Brîncoveanu**, E. Fiorentis, A. -M. Dumitrescu and M. M. Albu, "Metrici pentru evaluarea variabilității transferului de energie în rețelele electrice de distribuție" Revista Energetica – accepted to publication.